UNIVERSITY OF OKLAHOMA

GRADUATE COLLEGE

# Discovering Higgs Bosons of two Higgs doublet models with Bottom Quarks

A Dissertation

Submitted to the Graduate Faculty

in partial fulfillment of the requirements for the

degree of

Doctor of Philosophy

By

Shankar B. Sachithanandam
Norman, Oklahoma
2007

UMI Number: 3291244

UMI Microform 3291244



ProQuest Information and Learning Company
300 North Zeeb Road
P.O. Box 1346
Ann Arbor, MI 48106-1346

# Discovering Higgs Bosons of two Higgs doublet models with Bottom Quarks

A Dissertation Approved for the
Homer L. Dodge Department of Physics and Astronomy

By

Chung Kao (Chair)

Eric Abraham

Phillip Gutierrez

Ron Kantowski

Darryl McCullough

Kimball A. Milton

*Dedicated to my parents.*

# Contents

# List of Figures

# List of Tables

# Chapter 1

# Introduction

The Standard Model (SM) of elementary particles has so far successfully explained all known particle physics phenomena with remarkable precision [1]. The only evidence so far beyond the SM is the mass of the neutrino [2, 3] as well as dark matter [4, 5] and dark energy [6, 7].

## 1.1 Standard Model

Elementary particles are point like constituents of matter with no known substructure [8]. These elementary particles are the building blocks of matter known as matter particles and the intermediate interaction particles or gauge bosons.

The matter particles are fermions of spin $s = \frac{1}{2}$ and are classified into leptons and quarks. These are organized into three families. The particle content in each family is

$$1^{st} \text{ family: } \begin{pmatrix} \nu_e \\ e^- \end{pmatrix}_L, \; e^-_R, \; \begin{pmatrix} u \\ d \end{pmatrix}_L, \; u_R, \; d_R;$$

$$2^{nd} \text{ family: } \begin{pmatrix} \nu_\mu \\ \mu^- \end{pmatrix}_L, \; \mu^-_R, \; \begin{pmatrix} c \\ s \end{pmatrix}_L, \; c_R, \; s_R;$$

$$3^{rd} \text{ family: } \begin{pmatrix} \nu_\tau \\ \tau^- \end{pmatrix}_L, \; \tau^-_R, \; \begin{pmatrix} t \\ b \end{pmatrix}_L, \; t_R, \; b_R$$

and their corresponding anti-particles. The subscript $L$ and $R$ refer to the left and right handed chirality of the particles. The leptons, electron ($e^-$), muon ($\mu^-$), and tau ($\tau^-$) all

have an electric charge of $Q = -1$ and the corresponding neutrinos $\nu_e$, $\nu_\mu$, $\nu_\tau$ have $Q = 0$. The corresponding anti-particles have the same value of $Q$ except an opposite sign. All charges are given in terms of the elementary charge $e$ that is the charge of proton. The quarks are of six different flavors: three up-type quarks ($u$, $c$, $t$) and down-type quarks ($d$, $s$, $b$), with fractional charge $Q = \frac{2}{3}, -\frac{1}{3}, -\frac{1}{3}, \frac{2}{3}, -\frac{1}{3}$, and $\frac{2}{3}$ respectively.

All interactions excluding gravitational interactions are mediated by the exchange of an elementary particle that is a boson with spin $s = 1$. The photon $\gamma$ is the boson exchanged in electromagnetic interactions. There are eight gluons involved in strong interactions among quarks. $W^\pm$ or $Z$ are exchanged in electro-weak interactions. The photons and gluons are massless and charge-neutral while the $Z$ is massive and charge-neutral. $W^\pm$ are massive and have charge $Q = \pm\ 1$ respectively.

## 1.2 QED: Electromagnetic interactions

Quantum electrodynamics (QED) is the gauge theory of electromagnetic interactions. This is the most successful theory in particle physics and has been tested to very high precision.

To describe the gauge theory of electromagnetic interactions you start with the Lagrangian of a free Dirac field given by

$$\mathcal{L} = \bar{\Psi}(x)\,(i\,\partial\!\!\!/ - m)\,\Psi(x);\; \partial\!\!\!/ \equiv \partial_\mu \gamma^\mu$$

where $m$ is the mass of a fermion and $\gamma^\mu$ are the Dirac $\gamma$-matrices that obey the anti-commutation relation $\{\gamma^\mu, \gamma^\nu\} = 2\,g^{\mu\nu}$ where $g^{00} = 1$ and $g^{ij} = -1$ for $i = j$ and 0 otherwise.

Let us apply a global U(1) transformation to the Dirac field:

$$\Psi \rightarrow e^{i\,\theta\,Q}\Psi$$

where $\theta$ is the global phase with $\theta$ being the continuous parameter and $Q$ being the U(1) generator. If $Q$ and $\theta$ are space-time independent the Lagrangian remains invariant under this transformation.

When we make $\theta$ to be space-time dependent the Lagrangian is no longer invariant under this transformation. To make the Lagrangian invariant under such a transformation we need to introduce a vector field $A_\mu$. This field transforms such that the Lagrangian remains invariant under this local transformation. The vector field represents the photon field and its local U(1) transformation is given by

$$A_\mu \rightarrow A_\mu - \frac{1}{e}\partial_\mu\theta(x).$$

The compact way of writing the new gauge invariant Lagrangian is to replace the normal derivative with the so called covariant derivative

$$D_\mu\Psi \equiv (\partial_\mu - ieQA_\mu)\Psi.$$

Including the propagation term for the photon given by the gauge invariant field strength tensor

$$F_{\mu\nu} = \partial_\mu A_\nu - \partial_\nu A_\mu$$

the final Lagrangian for QED is given by

$$\boxed{\mathcal{L}_{QED} = \bar{\Psi}(x)(i\not{D} - m)\Psi(x) - \frac{1}{4}F_{\mu\nu}(x)F^{\mu\nu}(x).}$$

The interaction between the photon and the fermion field is in the $\bar{\Psi}i\not{D}\Psi$ term

$$\bar{\Psi}e\,Q A_\mu \gamma^\mu \Psi.$$

## 1.3 QCD: Strong Interactions

The gauge theory of strong interactions is based on the local symmetry of the non-Abelian SU(3) group. There are three possible color states for each quark flavor which form a triplet in the fundamental representation of SU(3). The gluons are the gauge bosons of the strong interaction and there are eight of them corresponding to eight generators of the SU(3) group.

The Lagrangian that is invariant under SU(3) transformation is given by

$$\mathcal{L}_{QCD} = \sum_q \bar{q}(x)(i\not{D} - m_q)q(x) - \frac{1}{4}F^\alpha_{\mu\nu}(x)F^{\mu\nu}_\alpha(x)$$

where

$$D_\mu q \equiv (\partial_\mu - ig_s(\frac{\lambda_\alpha}{2})G^\alpha_\mu)q;$$

$$q = \begin{pmatrix} q_1 \\ q_2 \\ q_3 \end{pmatrix}$$

and

$$q_i = \text{quark fields; } i = 1, 2, 3$$

$$g_s = \text{strong coupling constant}$$

$$\frac{\lambda_\alpha}{2} = \text{SU(3) generators}$$

$$G^\alpha_\mu = \text{gluon fields; } \alpha = 1, \ldots, 8.$$

The gluon field strength tensor is

$$F^\alpha_{\mu\nu}(x) = \partial_\mu G^\alpha_\nu(x) - \partial_\nu G^\alpha_\mu(x) + g_s f^{\alpha\beta\gamma} G_{\mu\beta} G_{\nu\gamma}.$$

The interaction term is found in the $\bar{q} i \not{D} q$ term. The gluons have self-interaction terms due to the non-Abelian nature of the SU(3) group.

## 1.4 SM: The Gauge theory of Electroweak interactions

The gauge theory of electroweak interactions is based on the local symmetry of the $\mathrm{SU}(2)_L \times \mathrm{U}(1)_Y$ group. This group has four generators. They are the three $\mathrm{SU}(2)_L$ generators $T_i = \frac{\sigma_i}{2}$ $i = 1, 2, 3$ with $\sigma_i$ being the three Pauli matrices and $\frac{Y}{2}$ being the $\mathrm{U}(1)_Y$ generator. The commutation relations for the total group are

$$[T_i, T_j] = i\,\epsilon_{ijk}\,T_k \;;\; [T_i, Y] = 0 \;;\; i, j, k = 1, 2, 3$$

and $\epsilon_{ijk} = +1$ under cyclic permutation of the indexes or -1 under anti-cyclic permutation and is zero otherwise. The Dirac field can be written as

$$\Psi = \Psi_L + \Psi_R;$$
$$\Psi_L = \left(\frac{1-\gamma_5}{2}\right)\Psi;$$
$$\Psi_R = \left(\frac{1+\gamma_5}{2}\right)\Psi$$

where $\Psi_L$ are the left handed fermions and $\Psi_R$ are the right handed fermions and $\gamma_5 = i\gamma_0\gamma_1\gamma_2\gamma_3$. The left-handed fields transform as doublets under $\mathrm{SU}(2)_L$ as

$$\Psi_L \rightarrow e^{i\theta^i T^i}\Psi_L$$

and the right-handed fermions transform as singlets.

The Lagrangian that is invariant under $\mathrm{SU}(2)_L \times \mathrm{U}(1)$ transformation is given by

$$\begin{aligned}
\mathcal{L}_G = &-\frac{1}{4}W^i_{\mu\nu}W^{\mu\nu}_i - \frac{1}{4}B^{\mu\nu}B_{\mu\nu} \\
&- \bar{\Psi}_L i\not{D}\Psi_L \\
&- \bar{\Psi}_R i\not{D}\Psi_R; \\
W^i_{\mu\nu} = &\ \partial_\mu W^i_\nu - \partial_\nu W^i_\mu + g\epsilon^{ijk}W^j_\mu W^k_\nu \text{ and} \\
B_{\mu\nu} = &\ \partial_\mu B_\nu - \partial_\nu B_\mu.
\end{aligned}$$

Unlike the $B_{\mu\nu}$ tensor which is similar to $F^{\mu\nu}$ in QED the $W^i_{\mu\nu}$ has a self-interacting term because of the non-Abelian nature of the SU(2) group.

The Lagrangian has been made invariant by introducing a covariant derivative similar to QED. In this case we need a separate covariant derivative for the left and right handed fields as they transform differently under SU(2).

As in the case of QED the interaction term comes from $\bar{\Psi}_{(L,R)} i \not{D} \Psi_{(L,R)}$ given by

$$\bar{\Psi}_L D_\mu \Psi_L = \bar{\Psi}_L(\partial_\mu - i\, g W_\mu^i T^i - i\, g' B_\mu \frac{Y}{2})\Psi_L$$

$$\text{and } \bar{\Psi}_R D_\mu \Psi_R = \bar{\Psi}_R(\partial_\mu - i\, g' B_\mu \frac{Y}{2})\Psi_R;$$

$$W_\mu^i T^i = W_\mu^+ T^+ + W_\mu^- T^- + W_\mu^3 T^3,$$

$$T^\pm = \frac{1}{2\sqrt{2}} \left(\sigma^1 \pm i\sigma^2\right),$$

$$\text{and } T^3 = \frac{\sigma^3}{2}.$$

The $\sigma$ s are the Pauli matrices. $g$ and $g'$ are the coupling constants of $\mathrm{SU}(2)_L$ and $\mathrm{U}(1)_Y$ groups .

Notice the absence of mass terms in the Lagrangian. The mass term in the Lagrangian written in terms of the left and right handed fields is

$$m\bar{\Psi}\Psi \;=\; m(\bar{\Psi}_L \Psi_R + \bar{\Psi}_R \Psi_L).$$

In QED the mass term in the Lagrangian is $m\psi\bar{\psi}$ because both the left and right-handed fields transform the same under U(1) transformation. This is not the case under $\mathrm{SU}(2)_L$ transformation because the left and right handed fields transform differently and so the mass term is forbidden under $\mathrm{SU}(2)_L$ transformations. The spontaneous breaking of this $\mathrm{SU}(2)_L \times \mathrm{U}(1)_Y$ transformation is achieved through the Higgs mechanism which will be

discussed in the next section.

We can get the physical gauge bosons $W^{\pm}$, Z and the photon by redefining the gauge fields as

$$\begin{pmatrix} W_\mu^3 \\ B_\mu \end{pmatrix} = \begin{pmatrix} \cos\theta_W & \sin\theta_W \\ -\sin\theta_W & \cos\theta_W \end{pmatrix} \begin{pmatrix} Z_\mu \\ A_\mu \end{pmatrix}$$

so that the boson fields can be written as

$$W_\mu^{\pm} = \frac{1}{\sqrt{2}}(W_\mu^1 \pm iW_\mu^2)$$

$$Z_\mu = \cos\theta_w - \sin\theta_w B_\mu$$

$$A_\mu = \sin\theta_w W_\mu^3 + \cos\theta_w B_\mu.$$

$A_\mu$ is the photon field and $\theta_W$ is the Weinberg angle for the mixing of the neutral sector.

## 1.5 The Higgs mechanism

All the particles remain massless to maintain gauge invariance. To generate particle masses in a gauge invariant way we need to introduce the Higgs mechanism. To generate masses for $Z$, $W^{\pm}$ and for the photon to remain massless we introduce a complex scalar doublet

$$\Phi = \begin{pmatrix} \phi^+ \\ \phi^0 \end{pmatrix}.$$

The quantum numbers of these fields are given in the table below. $T$ is the SU(2) generator or the weak isospin. $Y$ is the U(1) generator or weak hypercharge and $Q$ is the electric charge.

| | $T$ | $T^3$ | $\frac{Y}{2}$ | $Q$ |
|---|---|---|---|---|
| $\phi^+$ | $\frac{1}{2}$ | $\frac{1}{2}$ | $\frac{1}{2}$ | 1 |
| $\phi^0$ | $\frac{1}{2}$ | $-\frac{1}{2}$ | $\frac{1}{2}$ | 0 |

The Lagrangian for this field is

$$\mathcal{L} = (D_\mu \Phi)^\dagger (D^\mu \Phi) - V(\Phi);$$

$$V(\Phi) = \mu^2 \Phi^\dagger \Phi + \lambda (\Phi^\dagger \Phi)^2$$

where $\lambda > 0$ is the renormalizable scalar potential.

When we minimize the potential there are two possibilities for the vacuum expectation value (VEV): $\mu^2 > 0$ and $\mu^2 < 0$. For $\mu^2 > 0$ there is no $\mathrm{SU}(2)_L \times \mathrm{U}(1)_Y$ symmetry breaking and the vacuum does not acquire a VEV but in the latter case

$$|\langle 0|\Phi|0\rangle| = \begin{pmatrix} 0 \\ \frac{v}{\sqrt{2}} \end{pmatrix}; \; v \equiv \sqrt{\frac{-\mu^2}{\lambda}}.$$

To get the real fields $\vec{\xi}(x)$ and $H(x)$ whose VEV is zero we redefine $\Phi$ as

$$\Phi(x) = e^{\frac{i\vec{\xi}(x)\cdot\vec{\sigma}}{v}} \begin{pmatrix} 0 \\ \frac{H(x)+v}{\sqrt{2}} \end{pmatrix}.$$

To eliminate $\vec{\xi}(x)$ we do a local gauge transformation and rewrite the Lagrangian with

$$\Phi(x) = \begin{pmatrix} 0 \\ \dfrac{H(x)+v}{\sqrt{2}} \end{pmatrix}$$

and the covariant derivative

$$\begin{aligned} D_\mu &= \partial_\mu - igW_\mu^i T^i - \frac{1}{2}g' B_\mu \frac{Y}{2} \\ &= \partial_\mu - ig(W_\mu^+ T^+ + W_\mu^- T^-) \\ &- ieA_\mu Q - i\frac{g}{\cos\theta_W} Z_\mu (T^3 - \sin^2\theta_W Q). \end{aligned}$$

Since $Q = 0$ for $\phi^0$ all the terms with $Q$ vanish. Rewriting the Lagrangian in terms of the new $\Phi$ and the covariant derivative we have

$$\begin{aligned} \mathcal{L} = &\frac{1}{2}\partial_\mu H \partial^\mu H + \frac{g^2}{4}\left(W_\mu^+ W^{\mu-} + \frac{Z_\mu Z^\mu}{\cos^2\theta_W}\right)(H+v)^2 \\ &- V\left(\frac{H+v}{\sqrt{2}}\right). \end{aligned}$$

Expanding the scalar potential and isolating the $v^2$ terms we get the masses of $Z$, $W^\pm$ and the Higgs boson:

$$M_W = \frac{gv}{2},\ M_Z = \frac{gv}{2\cos\theta_W} \text{ and } M_H = \sqrt{-2\,\mu^2}.$$

The value of $v$ can be fixed from the measurement of the $W$ mass as in

$$v = 2\,\frac{M_W}{g}$$
$$\simeq 246\,\mathrm{GeV}.$$

The fermions are still massless and to generate the Fermion masses we introduce the Yukawa Lagrangian:

$$\mathcal{L}_{YW} = \lambda_e \bar{l}_L \Phi e_R + \lambda_u \bar{q}_L \tilde{\Phi} d_R + h.c. + \text{II and III families}$$

with

$$l_L = \begin{pmatrix} \nu_L \\ e_L \end{pmatrix} \; ; \; q_L = \begin{pmatrix} u_L \\ d_L \end{pmatrix} \text{ and } \tilde{\Phi} = i\sigma_2 \Phi^*.$$

As before the fermion masses can be generated by substituting

$$\Phi = \begin{pmatrix} 0 \\ \frac{v+H(x)}{2} \end{pmatrix}$$

which gives the fermion masses

$$m_e = \lambda_e \frac{v}{\sqrt{2}}; \; m_u = \lambda_u \frac{v}{\sqrt{2}} \text{ and } m_d = \lambda_d \frac{v}{\sqrt{2}}$$

where the $\lambda$ are the Yukawa couplings.

## 1.6 Experimental constraints on the Higgs boson mass

As we found in the previous section, the vacuum expectation value of the Higgs field can be determined by measuring the $W$ mass, the fine structure constant, and the weak mixing angle. The SM Higgs mass ($M_H = \sqrt{-2\,\mu^2}$) cannot be fixed because $\mu$ is a free parameter. Although the Higgs mass is a free parameter in the SM, indirect experimental limits can be set from precision measurements of electroweak parameters. The electroweak parameters depend on the Higgs mass logarithmically through radiative corrections. The combined direct searches of the four LEP experiments ALEPH, DELPHI, L3, and OPAL [9] set a lower bound of 114.4 GeV for the SM Higgs mass at the 95% confidence level.

Figure 1.1 shows $\Delta\chi^2 = \chi^2 - \chi^2_{min.}$ of the fit to all measurements as a function of $M_H$ [10]. The 95% confidence level upper limit on $M_H$ including the theoretical uncertainty in the Higgs mass due to higher order radiative corrections (shaded band) is 144 GeV. In calculating the upper limit of 144 GeV the lower limit from direct searches (vertical shaded region) has not been included. If the lower limit is included the upper limit increases to 182 GeV.

## 1.7 Theoretical constraints on the Higgs mass

Apart from the lower and upper limits to the SM Higgs mass from experiments theoretical considerations place bounds on the Higgs mass. We shall discus the upper bound on the Higgs mass due to unitarity considerations.

In the SM, the scattering amplitude for the process $W^+W^- \rightarrow W^+W^-$, without including the Higgs particle, grows with the center of mass energy ($\sqrt{s}$) thereby violating

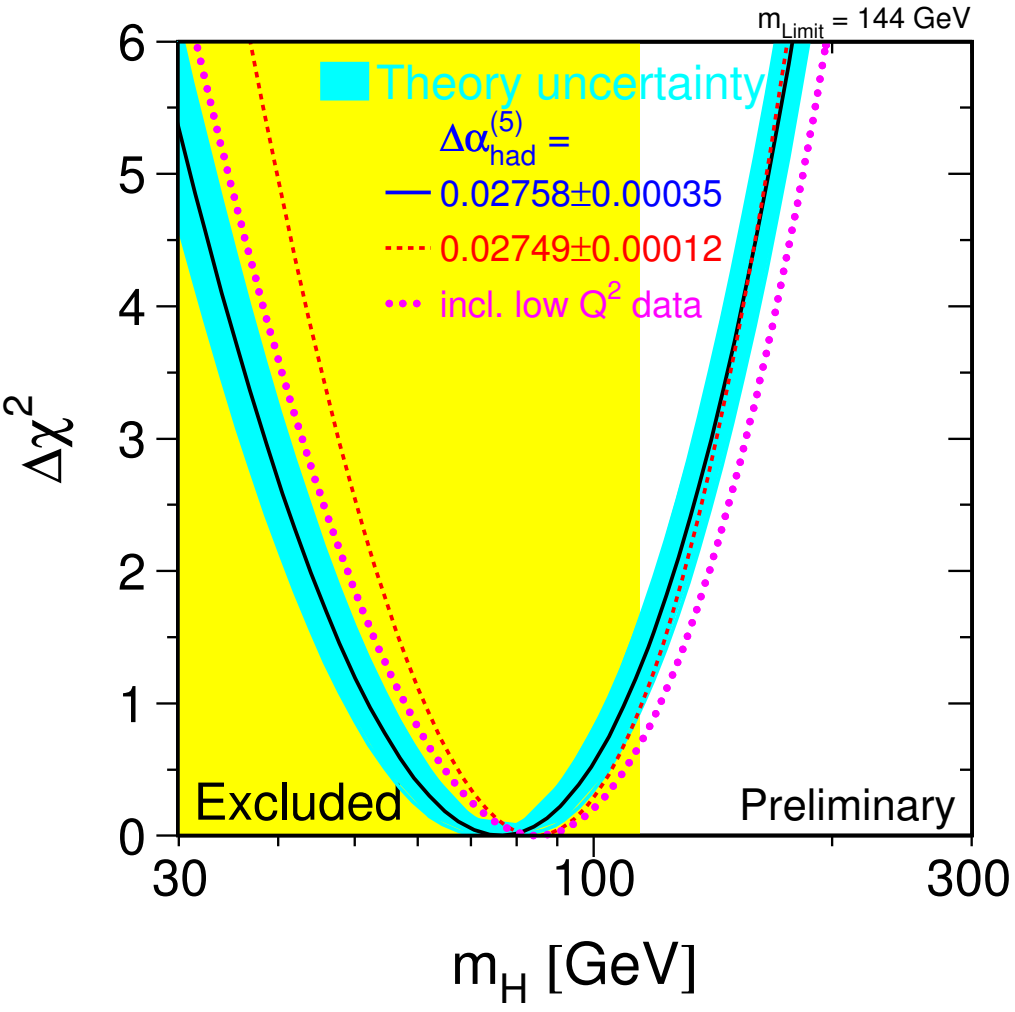


Figure 1.1: $\Delta\chi^2 = \chi^2 - \chi^2_{min.}$ The solid curve is the result of the fit of all Z-pole data plus direct measurements of $m_t$, $M_W$, and the $W$ decay width $\Gamma_W$ (high-$Q^2$ results). The band represents an estimate of the theoretical error due to higher order corrections. The vertical shaded region shows the 95% CL exclusion limit on $m_H$ from direct searches. $\Delta\alpha^{(5)}_{\rm had}$ is the contribution of light quarks to the photon vacuum polarization. The low-$Q^2$ data is from atomic parity violation, $e^-e^-$ Moller scattering, and neutrino-nucleon scattering.

unitarity. The inclusion of the Higgs particle cancels the terms that grow with $s$ resulting in a finite value for the scattering amplitude, but if $M_H \to \infty$ the unitarity violating terms reappear. To illustrate how $M_H \to \infty$ violates unitarity let us calculate the amplitude for the elastic scattering of the $W$ bosons [11]. As $s$ becomes large the $W$ bosons become longitudinally polarized. The scattering amplitude when $s,\ M_H^2 \gg M_W^2,\ M_Z^2$ is

$$\mathcal{A}\left(W_L^+ W_L^- \to W_L^+ W_L^-\right) = -\sqrt{2}\, G_F\, M_H^2 \left[\frac{s}{s - M_H^2} + \frac{t}{t - M_H^2}\right]$$

where $G_F$ is the Fermi constant, $s$ and $t$ are the Mandelstam variables. The above expression shows that the scattering amplitude is linearly dependent on $s$ when $M_H^2 \to \infty$, but even if $M_H$ is finite the scattering amplitude may violate unitarity. This behavior can be shown by calculating the scattering amplitude contribution to the partial wave $a_J$ with $J = 0$ or zero total angular momentum. The partial wave for $J = 0$ is

$$\begin{aligned} a_0 &= \frac{1}{16\,\pi\, s} \int_{-s}^{0} \mathcal{A}\left(W_L^+ W_L^- \to W_L^+ W_L^-\right) \mathrm{d}t \\ &= -\frac{G_F\, M_H^2}{8\,\pi\,\sqrt{2}} \left[2 + \frac{M_H^2}{s - M_H^2} - \frac{M_H^2}{s} \ln\left(1 + \frac{s}{M_H^2}\right)\right] \end{aligned}$$

and for $s \gg M_H^2$

$$a_0 = -\frac{G_F\, M_H^2}{4\,\pi\,\sqrt{2}}.$$

Partial wave unitarity requires

$$|a_0|^2 \leq |\mathrm{Im}\, a_0|$$

which implies $|a_0| \leq 1$ and

$$(\,\mathrm{Re}\, a_0\,)^2 \;\leq\; |\mathrm{Im}\, a_0|\;(\,1 \,-\, |\mathrm{Im}\, a_0|\,)\,.$$

The right-hand side of the above expression has an upper limit of $1/4$ resulting in the condition:

$$|\,\mathrm{Re}\, a_0\,| \;\leq\; \frac{1}{2}.$$

These conditions result in an upper bound for the Higgs mass $M_H < 850$ GeV [12].

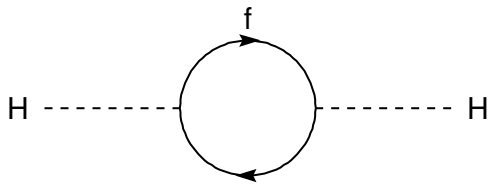


Figure 1.2: The one-loop contribution of a fermion $f$ to the Higgs boson mass.

## 1.8 TeV scale and New Physics

Having established that the favored SM Higgs mass is in the range 114.4 GeV $\lesssim m_H \lesssim$ 182 GeV from experimental considerations, and $M_H < 850$ GeV to preserve unitarity, we now discuss the need for new models beyond the SM at the TeV scale. Although SM is a renormalizable quantum field theory that can be used to evaluate radiative corrections to any precision it is doubtful if the theory can be effective up to the Planck scale $M_P \sim 10^{19}$ GeV. For example when we calculate the radiative corrections to the SM Higgs mass we encounter quadratic divergences in the cut-off scale $\Lambda$.

To illustrate this problem let us calculate the one-loop contributions to the Higgs mass from a fermion $f$ in figure 1.2. The fermion one-loop contribution to the Higgs mass is

$$\Delta M_H^2 \;=\; -\frac{\lambda_f^2}{8\pi^2}\left[\Lambda^2 - 6\,m_f^2\,\ln\left(\frac{\Lambda}{m_f}\right) \;+\; 2\,m_f^2\right] \;+\; \mathcal{O}(1/\Lambda^2)$$

where $\lambda_f = \sqrt{2}\,m_f/v$ is the Yukawa coupling and for simplicity the external Higgs momentum squared is neglected by assuming the fermion to be massive [13]. The first term in the expression above is quadratic in the cut-off scale $\Lambda$ and the second term is logarithmic in $\Lambda$. If $\Lambda$ is chosen to be either the GUT scale $10^{16}$ GeV or the Planck scale $10^{19}$ GeV

the contribution from the quadratic term is very large while the logarithmic contribution is small. As described in the previous section the SM Higgs mass is expected to be around 200 GeV, and for the SM Higgs mass to be in the 100 to 200 GeV range we have to add a counter-term to the mass squared and adjust it with a precision of $\mathcal{O}(10^{-30})$ which seems unnatural. This is known as the naturalness problem [14].

Supersymmetry provides a framework to overcome this problem. Now let us assume that there exists a scalar particle $S$ with mass $m_S$. The radiative correction to the Higgs mass from the loop diagrams of the scalar particle $S$ in figure 1.3 is

$$\Delta M_H^2 \;=\; \frac{\lambda_S}{16\pi^2}\left[\Lambda^2 - 2\,m_S^2\,\ln\left(\frac{\Lambda}{m_S}\right)\right] \;+\; \frac{\lambda_S^2}{16\,\pi^2}\,v^2\left[1 - 2\,\ln\left(\frac{\Lambda}{m_S}\right)\right] \;+\; \mathcal{O}(1/\Lambda^2)$$

where $\lambda_S$ is the quadlinear Higgs coupling to the scalar particle. If we make the assumption that each fermion in the SM is accompanied by two scalars with $\lambda_S = |\lambda_f|^2$ then the quadratic divergence due to the scalar loop exactly cancels the fermion loop contribution [15]. This is possible due to the relative minus sign between the fermion loop and the boson loop contributions to $\Delta M_H^2$. The mass correction to the Higgs particle from both the scalar and fermion loop contributions is

$$\Delta M_H^2 \;=\; \frac{\lambda_f^2}{4\pi^2}\left[(m_f^2 - m_S^2)\,\log\left(\frac{\Lambda}{m_S}\right) \;+\; 3\,m_f^2\,\log\left(\frac{m_S}{m_f}\right)\right] \;+\; \mathcal{O}(1/\Lambda^2).$$

The counter-term adjusted to a precision of $\mathcal{O}(10^{-30})$ that was required earlier to cancel the quadratic divergences is not required anymore. This symmetry that relates the fermions and bosons is known as Supersymmetry. Supersymmetry is not an exact symmetry because scalar particles with the same mass as fermions have not been found. If this symmetry is

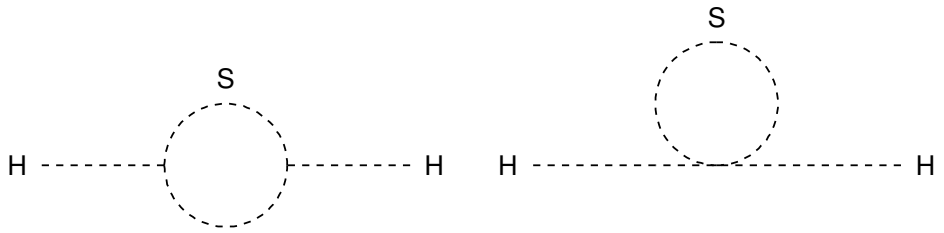


Figure 1.3: The one-loop contributions of the scalar particle $S$ to the Higgs boson mass.

badly broken and the masses of the scalar particles are much larger than the fermions the quadratic divergences reappear because the correction $\Delta M_H^2$ is proportional to $m_f^2 - m_S^2$. To prevent the quadratic divergences from reappearing and to keep the SM Higgs mass at the electroweak symmetry breaking scale the new scalar particles should not be much heavier than a few TeV [16].

The Large Hadron Collider (LHC) which will be operational with a center of mass energy $\sqrt{s} = 14$ TeV should be able to detect the SM Higgs and the supersymmetric particles if they exist [17, 18]. If the SM Higgs mass is below 200 GeV the Tevatron ($\sqrt{s} = 2$ TeV) should be able to detect the SM Higgs [19].

## Chapter 2

# The Two Higgs Doublet Models

In this chapter we describe the general properties of the two Higgs doublet models [11] and the minimal supersymmetric extension of the Standard Model (MSSM). In the general two Higgs doublet models, two Higgs doublets are required to give mass to the up-type and down-type quarks and the corresponding leptons [20, 21]. The two doublets have eight degrees of freedom giving rise to three Goldstone bosons and five real Higgs bosons. There is a charged pair, two neutral and a pseudoscalar Higgs.

In this thesis we use the general two Higgs Doublet model (2HDM) without any reference to supersymmetry and the MSSM where the scalar-quark and scalar-lepton fields do not acquire any vacuum expectation values. We focus on the three neutral Higgs and their discovery potential at the LHC through fusion of gluons and bottom quarks.

## 2.1 The General Two Higgs Doublet Model

In the 2HDM there are two $\mathrm{SU}(2)_L$ complex doublet scalar fields $\Phi_1$ and $\Phi_2$ instead of a single doublet complex scalar field in the SM. The complex doublet fields are

$$\Phi_1 = \begin{pmatrix} \Phi_1^+ \\ \\ \Phi_1^0 \end{pmatrix} \text{ and } \Phi_2 = \begin{pmatrix} \Phi_2^+ \\ \\ \Phi_2^0 \end{pmatrix}.$$

The quantum numbers of these fields are given in the table below.

$T$ is the SU(2) generator or the weak isospin. $Y$ is the hypercharge or U(1) generator and $Q$ is the electric charge. We note that the quantum numbers of both the doublet fields

| | $T$ | $T^3$ | $\frac{Y}{2}$ | $Q$ |
|---|---|---|---|---|
| $\Phi_1^+$ | $\frac{1}{2}$ | $\frac{1}{2}$ | $\frac{1}{2}$ | 1 |
| $\Phi_1^0$ | $\frac{1}{2}$ | $-\frac{1}{2}$ | $\frac{1}{2}$ | 0 |

| | $T$ | $T^3$ | $\frac{Y}{2}$ | $Q$ |
|---|---|---|---|---|
| $\Phi_2^+$ | $\frac{1}{2}$ | $\frac{1}{2}$ | $\frac{1}{2}$ | 1 |
| $\Phi_2^0$ | $\frac{1}{2}$ | $-\frac{1}{2}$ | $\frac{1}{2}$ | 0 |

is the same as the SM doublet field which will not be the case in MSSM.

In this model the Higgs potential that spontaneously breaks $\mathrm{SU}(2)_L \times \mathrm{U}(1)_Y$ down to $\mathrm{U}(1)_{\mathrm{EM}}$ can be written as [22]

$$\begin{aligned} V(\Phi_1,\, \Phi_2) \; =& \lambda_1(\Phi_1^\dagger\Phi_1 - v_1^2)^2 + \lambda_2(\Phi_2^\dagger\Phi_2 - v_2^2)^2 \\ &+ \lambda_3\left[(\Phi_1^\dagger\Phi_1 - v_1^2) + (\Phi_2^\dagger\Phi_2 - v_2^2)\right]^2 \\ &+ \lambda_4\left[(\Phi_1^\dagger\Phi_1)(\Phi_2^\dagger\Phi_2) - (\Phi_1^\dagger\Phi_2)(\Phi_2^\dagger\Phi_1)\right] \\ &+ \lambda_5\left[\mathrm{Re}\,(\Phi_1^\dagger\Phi_2) - v_1 v_2\cos\xi\right]^2 \\ &+ \lambda_6\left[\mathrm{Im}\,(\Phi_1^\dagger\Phi_2) - v_1 v_2\sin\xi\right]^2 \end{aligned}$$

where the $\lambda_i$ are all real parameters.

The Lagrangian of the doublet fields can be written as

$$\mathcal{L} = (D_\mu\Phi_1)^\dagger(D^\mu\Phi_1) + (D_\mu\Phi_2)^\dagger(D^\mu\Phi_2) - V(\Phi_1, \Phi_2).$$

The vacuum expectation values that break the symmetry is given by

$$\langle \Phi_1 \rangle = \begin{pmatrix} 0 \\ \\ v_1 \end{pmatrix} \text{ and } \langle \Phi_2 \rangle = \begin{pmatrix} 0 \\ \\ v_2 e^{\imath \xi} \end{pmatrix}.$$

If we require $\lambda_5 = \lambda_6$ the last two terms can be combined and written as $\left| \Phi_1^\dagger \Phi_2 - v_1 v_2 e^{\imath \xi} \right|^2$ and the phase factor $\xi$ can be removed by a global gauge transformation resulting in real vacuum expectation values. Eliminating $\xi$ makes it the most general $CP$ conserving model which is the model studied in this thesis.

The Higgs boson mass matrix is most easily done in the real basis [23, 24]. Let the fields be defined as

$$\Phi_1 \equiv \begin{pmatrix} \Phi_1^\dagger \\ \\ \Phi_1^0 \end{pmatrix} = \begin{pmatrix} \phi_1 + \imath \phi_2 \\ \\ \phi_3 + \imath \phi_4 \end{pmatrix} \rightarrow \begin{pmatrix} \phi_1 \\ \\ \phi_2 \\ \\ \phi_3 \\ \\ \phi_4 \end{pmatrix}$$

and

$$\Phi_2 \equiv \begin{pmatrix} \Phi_2^\dagger \\ \\ \Phi_2^0 \end{pmatrix} = \begin{pmatrix} \phi_5 + \imath \phi_6 \\ \\ \phi_7 + \imath \phi_8 \end{pmatrix} \rightarrow \begin{pmatrix} \phi_5 \\ \\ \phi_6 \\ \\ \phi_7 \\ \\ \phi_8 \end{pmatrix}.$$

The matrix elements of the Higgs boson squared mass matrix is given by

$$M_{ij}^2 = \frac{1}{2} \frac{\partial^2 V}{\partial \phi_i \partial \phi_j} \bigg|_{\text{min.}}$$

where the minimum is the vacuum expectation of the fields $\phi_i$ and $\phi_j$ with $i,\ j = 1$ to 8. The vacuum expectation values of all the fields are zero except $\langle\phi_3\rangle = v_1$ and $\langle\phi_7\rangle = v_2$.

By diagonalizing the mass matrices we get the physical Higgs states and the unphysical Goldstone states. The charged Goldstone states and the corresponding charged Higgs states are

$$G^{\pm} = \Phi_1^{\pm}\cos\beta + \Phi_2^{\pm}\sin\beta,$$

$$H^{\pm} = -\Phi_1^{\pm}\sin\beta + \Phi_2^{\pm}\cos\beta$$

with $\tan\beta = \frac{v_2}{v_1}$ and the Higgs masses being $m^2_{H^{\pm}} = \lambda_4\,(v_1^2 + v_2^2)$. The neutral Goldstone boson state is

$$G^0 = \sqrt{2}\,(\mathrm{Im}\,\Phi_1^0\cos\beta + \mathrm{Im}\,\Phi_2^0\sin\beta)$$

and the physical pseudoscalar state is

$$A^0 = \sqrt{2}\,(-\mathrm{Im}\,\Phi_1^0\sin\beta + \mathrm{Im}\,\Phi_2^0\cos\beta)$$

with mass $m^2_{A^0} = \lambda_6\,(v_1^2 + v_2^2)$. The two neutral $CP$-even Higgs scalars are mixed through the matrix

$$\mathcal{M} = \begin{pmatrix} 4v_1^2(\lambda_1+\lambda_3) + v_2^2\lambda_5 & (4\lambda_3+\lambda_5)v_1v_2 \\ (4\lambda_3+\lambda_5)v_1v_2 & 4v_2^2(\lambda_1+\lambda_3) + v_1^2\lambda_5 \end{pmatrix}.$$

The Higgs eigenstates and their masses are

$$\begin{aligned} H^0 =& \sqrt{2}\left[(\mathrm{Re}\,\Phi_1^0 - v_1)\cos\alpha + (\mathrm{Re}\,\Phi_2^0 - v_2)\sin\alpha\right], \\ h^0 =& \sqrt{2}\left[-(\mathrm{Re}\,\Phi_1^0 - v_1)\sin\alpha + (\mathrm{Re}\,\Phi_2^0 - v_2)\cos\alpha\right], \\ m^2_{H^0,h^0} =& \frac{1}{2}\left[\mathcal{M}_{11} + \mathcal{M}_{22} \pm \sqrt{(\mathcal{M}_{11} - \mathcal{M}_{22})^2 + 4\mathcal{M}_{12}^2}\right] \end{aligned}$$

and the mixing angle is

$$\begin{aligned} \sin 2\alpha =& \frac{2\mathcal{M}_{12}}{\sqrt{(\mathcal{M}_{11} - \mathcal{M}_{22})^2 + 4\mathcal{M}_{12}^2}}, \\ \cos 2\alpha =& \frac{\mathcal{M}_{11} - \mathcal{M}_{22}}{\sqrt{(\mathcal{M}_{11} - \mathcal{M}_{22})^2 + 4\mathcal{M}_{12}^2}}. \end{aligned}$$

Four Higgs masses, the ratio of the vacuum expectation values ($\tan\beta = \frac{v_2}{v_1}$), and the mixing angle $\alpha$ are all free parameters. In the Standard Model the vacuum expectation value is fixed by the $W$ mass $M_W^2 = \frac{g^2 v^2}{4}$ where $g$ is the SU(2) gauge coupling. Similarly in the general Two Higgs Model $M_W^2 = \frac{g^2(v_1^2 + v_2^2)}{4}$ is the constraint on the vacuum expectation values $v_1$ and $v_2$ .

Rewriting the Higgs fields in terms of the $\Phi$ fields in the unitary gauge, we get

$$\begin{aligned} \Phi_1^{\pm} &= -H^{\pm}\sin\beta \\ \Phi_2^{\pm} &= H^{\pm}\cos\beta \\ \Phi_1^0 &= v_1 + \frac{1}{\sqrt{2}}(H^0\cos\alpha - h^0\sin\alpha + \imath A^0\sin\beta) \\ \Phi_2^0 &= v_2 + \frac{1}{\sqrt{2}}(H^0\sin\alpha + h^0\cos\alpha + \imath A^0\cos\beta). \end{aligned}$$

$\Phi^- = (\Phi^+)^*$ and $*$ refers to complex conjugation.

In this study we use the Model II Yukawa interactions [25] in which one Higgs doublet ($\Phi_1$) couples only to the down-type quarks and leptons and the other Higgs doublet ($\Phi_2$) couples only to up-type quarks. The Higgs-fermion interaction Lagrangian for this model is

$$\begin{aligned}\mathcal{L}_{Hf\bar{f}} = &- \frac{g}{2m_W \cos\beta}\bar{D}M_D D(H^0\cos\alpha - h^0\sin\alpha) + \frac{\imath g\tan\beta}{2m_W}\bar{D}M_D\gamma_5 D A^0 \\ &- \frac{g}{2m_W \sin\beta}\bar{U}M_U U(H^0\sin\alpha + h^0\cos\alpha) + \frac{\imath g\cot\beta}{2m_W}\bar{U}M_U\gamma_5 U A^0 \\ &+ \frac{g}{2\sqrt{2}m_W}(H^+\bar{U}\left[\cot\beta M_U K(1-\gamma_5) + \tan\beta K M_D(1+\gamma_5)\right]D + h.c.).\end{aligned}$$

$U$ and $D$ are the column matrices of the three generations of up and down-type quarks. $M_U$ and $M_D$ are the diagonal mass matrices. $K$ is the Kobayashi-Maskawa mixing matrix. $\tan\beta \equiv v_2/v_1$ where $v_1$ ($v_2$) is the vacuum expectation value of the Higgs field which couples only to down-type (up-type) quarks. The lepton couplings are obtained by simply replacing the quark fields with the corresponding lepton fields and the mass matrices with the diagonal lepton mass matrices by setting the K-M matrix $K$ to the identity matrix.

The Lagrangian for the Higgs-gauge boson interaction is [23, 24]

$$\mathcal{L}_{\text{int}} = \mathcal{L}_{HHV} + \mathcal{L}_{HVV} + \mathcal{L}_{HHVV}$$

where

$$\begin{aligned}
\mathcal{L}_{HHV} =& -\frac{1}{2}\imath\, g\, W_\mu^+\, H^-\, \overset{\leftrightarrow}{\partial^\mu}\, [H^0 \sin(\alpha-\beta) + h^0 \cos(\alpha-\beta) + \imath A^0] + \text{h.c.} \\
& - \frac{\imath g}{2\cos\theta_W}\, Z_\mu \{\imath A^0\, \overset{\leftrightarrow}{\partial^\mu}\, [H^0 \sin(\alpha-\beta) + h^0 \cos(\alpha-\beta)] \\
& - (2\sin^2\theta_W - 1) H^- \overset{\leftrightarrow}{\partial^\mu} H^+\} - \imath e A_\mu\, H^- \overset{\leftrightarrow}{\partial^\mu} H^+ \\
\mathcal{L}_{HVV} =& \, g\, m_W W_\mu W^\mu [H^0 \cos(\beta-\alpha) + h^0 \sin(\beta-\alpha)] \\
& + \frac{g m_Z}{2\cos\theta_W} Z_\mu Z^\mu [H^0 \cos(\beta-\alpha) + h^0 \sin(\beta-\alpha)] \\
\mathcal{L}_{HHVV} =& \frac{1}{2} g^2 W_\mu W^\mu [(H^0)^2 + (h^0)^2 + (A^0)^2 + 2H^+H^-] \\
& + \frac{g^2}{8\cos^2\theta_W} Z_\mu Z^\mu [(H^0)^2 + (h^0)^2 + (A^0)^2 + 2\cos^2\theta_W H^+H^-] \\
& + e^2 A_\mu A^\mu H^+H^- + \frac{eg\cos 2\theta_W}{\cos\theta_W} A_\mu Z^\mu H^+H^- \\
& - \frac{g}{2}\left(eA^\mu - \frac{g\sin^2\theta_W}{\cos\theta_W} Z^\mu\right) \\
& \times \{W_\mu^+ H^- [H^0 \sin(\beta-\alpha) - h^0\cos(\beta-\alpha) - \imath A^0] + h.c.\}.
\end{aligned}$$

For completeness we have given the interaction term for the charged Higgs fields.

Let us examine the Higgs-quark couplings relative to the minimal SM values using the third family of quarks as an example:

$$H^0 t\bar{t} : \frac{\sin\alpha}{\sin\beta} \qquad H^0 b\bar{b} : \frac{\cos\alpha}{\cos\beta}$$

$$h^0 t\bar{t} : \frac{\cos\alpha}{\sin\beta} \qquad h^0 b\bar{b} : \frac{-\sin\alpha}{\cos\beta}$$

$$A^0 t\bar{t} : \cot\beta\,\gamma_5 \quad A^0 b\bar{b} : \tan\beta\,\gamma_5.$$

The $A^0 b\bar{b}$ coupling is enhanced for $\tan\beta > 1$ while the $A^0 t\bar{t}$ coupling is suppressed. For $\tan\beta < 1$ the $A^0 b\bar{b}$ coupling is suppressed and the top quark couplings are enhanced. Similar results hold for $H^0$ and $h^0$ except the mixing angle might reduce the strength of the coupling. The enhancement in the bottom quark couplings for large $\tan\beta$ values increases the discovery potential of the Higgs decaying into a $b\bar{b}$ pair in the two Higgs doublet models compared to the SM.

The Higgs-Higgs-gauge boson couplings are new because they do not appear in the SM. The couplings in the neutral sector are given by

$$g_{HAZ} = -\frac{g\sin(\beta-\alpha)}{2\cos\theta_W}(p_A + p_H)^\mu$$
$$g_{hAZ} = \frac{g\cos(\beta-\alpha)}{2\cos\theta_W}(p_A + p_h)^\mu$$

where the $p$ are the four momentum of the Higgs bosons. If we ignore the momentum term then we have

$$g^2_{HAZ} + g^2_{hAZ} = \frac{g^2}{4\cos\theta_W}.$$

Since there is no corresponding coupling in the SM we cannot make a comparison. However the sum of the couplings is equal to the SM $HVV$ coupling where V represents a massive gauge boson.

The $HVV$ coupling of the model relative to the SM is given by

$$\frac{g_{hVV}}{g_{SM}} = \sin(\beta - \alpha)$$
$$\frac{g_{HVV}}{g_{SM}} = \cos(\beta - \alpha).$$

Squaring and summing the terms we get

$$g^2_{hVV} + g^2_{HVV} = g^2_{SM}$$

which implies the Higgs coupling in the two Higgs doublet model is suppressed compared to the SM.

## 2.2 The Minimal Supersymmetric Standard Model

In the minimal Standard Model only one Higgs doublet is required to give mass to both quarks and leptons. In contrast the supersymmetric models require *two* Higgs doublet models to give mass to both up-type and down-type quarks and the corresponding leptons [20, 21, 26].

In the MSSM used in our study we assume that the scalar-quark and scalar-lepton fields do not acquire vacuum expectation values. Let $H_1$ and $H_2$ be the two scalar doublet fields. Their quantum numbers are given in the table below.

| | $T$ | $T^3$ | $\frac{Y}{2}$ | $Q$ |
|---|---|---|---|---|
| $H_1^1$ | $\frac{1}{2}$ | $\frac{1}{2}$ | $-\frac{1}{2}$ | 0 |
| $H_1^2$ | $\frac{1}{2}$ | $-\frac{1}{2}$ | $-\frac{1}{2}$ | $-1$ |

| | $T$ | $T^3$ | $\frac{Y}{2}$ | $Q$ |
|---|---|---|---|---|
| $H_2^1$ | $\frac{1}{2}$ | $-\frac{1}{2}$ | $\frac{1}{2}$ | 0 |
| $H_2^2$ | $\frac{1}{2}$ | $\frac{1}{2}$ | $\frac{1}{2}$ | 1 |

$T$ is the weak isospin. $Y$ is the hypercharge and $Q$ the electric charge. The relationship between $T$, $Y$, and $Q$ is $Q = T^3 + \frac{Y}{2}$. From the table we see that $H_1$ and $H_2$ have opposite hypercharges and this assignment of hypercharges constrains each Higgs field to give mass to either up-type or down-type quarks. For example an $H_1 Q_L U_R$ coupling where $Q_L$ is a quark doublet and $U_R$ is an up-type singlet field is prohibited because this term is not invariant under a U(1) transformation and therefore the up-type quarks will remain massless if $H_2$ is absent.

Since we are assuming that the fields of the supersymmetric partners do not acquire VEV and that there is no mixing between the singlet and doublet fields we can use all the results from the previous section. The resulting potential for this minimal model is

$$V = (m_1^2 + |\mu|^2) H_1^{i*} H_1^i + (m_2^2 + |\mu|^2) H_2^{i*} H_2^i - m_{12}^2 (\epsilon_{ij} H_1^i H_2^j + h.c.) \\ + \frac{1}{8}(g^2 + g'^2) \left[ H_1^{i*} H_1^i - H_2^{j*} H_2^j \right]^2 + \frac{1}{2} |H_1^{i*} H_2^i|^2.$$

The $H_1$ and $H_2$ fields in terms of the $\Phi$ fields of the previous section are

$$H_1 = \begin{pmatrix} H_1^1 \\ \\ H_1^2 \end{pmatrix} \equiv \begin{pmatrix} \Phi_1^{0*} \\ \\ -\Phi_1^- \end{pmatrix}$$

$$H_2 = \begin{pmatrix} H_2^1 \\ \\ H_2^2 \end{pmatrix} \equiv \begin{pmatrix} \Phi_2^+ \\ \\ \Phi_2^0 \end{pmatrix}.$$

$\Phi_1^- \equiv (\Phi_1^+)^*$ and the $*$ refers to complex conjugation.

The Higgs doublet fields $H_1$ and $H_2$ acquire vacuum expectation values given by

$$\langle H_1 \rangle = \begin{pmatrix} v_1 \\ \\ 0 \end{pmatrix} \text{ and } \langle H_2 \rangle = \begin{pmatrix} 0 \\ \\ v_2 \end{pmatrix}.$$

The Higgs doublet fields $H_1$ and $H_2$ written in terms of the physical Higgs and the Goldstone bosons are

$$H_2^1 = H^+ \cos\beta + G^+ \sin\beta$$

$$H_1^2 = H^- \sin\beta - G^- \cos\beta$$

$$H_1^1 = v_1 + \frac{1}{\sqrt{2}}(H^0 \cos\alpha - h^0 \sin\alpha + \imath A^0 \sin\beta - \imath G^0 \cos\beta)$$

$$H_2^2 = v_2 + \frac{1}{\sqrt{2}}(H^0 \sin\alpha + h^0 \cos\alpha + \imath A^0 \cos\beta - \imath G^0 \sin\beta).$$

As in the previous section $\alpha$ is the mixing angle and $\tan\beta$ is the ratio of the vacuum expectation values $v_1$ and $v_2$. The minimization constraints that are required to give non-zero values to $v_1$ and $v_2$ result in various relations between the parameters in the scalar potential. These parameters can be related to the $\lambda_i$ of the two Higgs field described in the

previous section as [24]

$$\begin{aligned}
\lambda_2 &= \lambda_1 \\
\lambda_3 &= \frac{1}{8}(g^2 + g'^2) - \lambda_1 \\
\lambda_4 &= 2\lambda_1 - \frac{1}{2}g'^2 \\
\lambda_5 &= \lambda_6 = 2\lambda_1 - \frac{1}{2}(g^2 + g'^2) \\
m_1^2 &= -|\mu|^2 + 2\lambda_1 v_2^2 - \frac{1}{2}m_Z^2 \\
m_2^2 &= -|\mu|^2 + 2\lambda_1 v_1^2 - \frac{1}{2}m_Z^2 \\
m_{12}^2 &= -\frac{1}{2}v_1 v_2(g^2 + g'^2 - 4\lambda_1).
\end{aligned}$$

Since $v_1$ and $v_2$ are greater than zero we can choose $0 \leq \beta \leq \pi/2$. Due to the minimization constraints we can choose only two independent parameters. We choose $\tan\beta$ and $m_A$. All the other Higgs masses and the mixing angle can now be calculated. The Higgs masses are given by

$$\begin{aligned}
m_{H^\pm}^2 &= m_{A^0}^2 + m_W^2 \\
m_{H^0,\,h^0}^2 &= \frac{1}{2}\left[m_{A^0}^2 + m_Z^2 \pm \sqrt{(m_{A^0}^2 + m_Z^2)^2 - 4m_Z^2 m_{A^0}^2 \cos^2 2\beta}\right].
\end{aligned}$$

The mixing angle $\alpha$ can be calculated from

$$\cos 2\alpha = -\cos 2\beta \left( \frac{m_{A^0}^2 - m_Z^2}{m_{H^0}^2 - m_{h^0}^2} \right)$$

$$\sin 2\alpha = -\sin 2\beta \left( \frac{m_{H^0}^2 + m_{h^0}^2}{m_{H^0}^2 - m_{h^0}^2} \right).$$

Analyzing the mass relationships we see that $m_{H^\pm} \geq m_W$, $m_{H^0} \geq m_Z$, $m_{A^0} \geq m_{h^0}$, and a constraint on $h^0$ given by

$$m_{h^0} \leq m|\cos 2\beta| \leq m_Z$$

$$m \equiv \min\{m_Z, m_{A^0}\}.$$

The maximum value of the Higgs mass reaches 135 GeV when radiative corrections are included. This upper bound on the mass of the light Higgs does not exist in the SM Higgs mass which is not bounded at the tree level. This important difference arises because the Higgs self-coupling in SM is proportional to a free parameter whereas the MSSM Higgs self-coupling is proportional to the square of the electroweak gauge couplings.

In summary, the Higgs sector of a 2HDM has six free parameters compared to one free parameter in the SM. The six parameters are the four Higgs masses and the ratio of the vacuum expectation values ($\tan\beta$) and a mixing angle $\alpha$. In contrast, the Higgs sector of the MSSM has only two free parameters and we choose them to be $m_A$ and $\tan\beta$. Once these values are fixed all the other parameters can be obtained. The Higgs-fermion

coupling depends on $\tan\beta$ and the $b\bar{b}$ coupling is enhanced at large $\tan\beta$ values while the $t\bar{t}$ coupling is suppressed compared to the SM couplings. For smaller $\tan\beta$ values the $t\bar{t}$ coupling is enhanced and the $b\bar{b}$ coupling is suppressed. The Higgs-gauge boson couplings are suppressed compared to the SM couplings. The enhancement of the bottom quark coupling for large $\tan\beta$ values will be exploited in studying the discovery potential of the pseudoscalar boson ($A^0$) in bottom quark fusion which we will be describing in the next chapter.

# Chapter 3

# Detecting a Higgs Pseudoscalar with a Z boson in Bottom Quark Fusion

## 3.1 Introduction

The four LEP collaborations ALEPH, DELPHI, L3 and OPAL have set a lower bound of 92.9 GeV and 93.4 GeV at the 95% confidence level for the lightest neutral Higgs mass ($h^0$) and the pseudoscalar Higgs ($A^0$) respectively [27]. There have been extensive studies done for the detection of a heavier MSSM Higgs boson ($\phi^0 = H^0 \text{ or } A^0$) at the CERN Large Hadron Collider (LHC) [17, 18, 28–37]. In this chapter we present the prospects of the discovery of a Higgs pseudoscalar associated with a $Z$ boson through the process $pp \to ZA^0 \to l\bar{l}b\bar{b} + X$ via the bottom quark fusion ($b\bar{b} \to ZA^0$) at the LHC [38].

## 3.2 Parton Distribution Functions

To calculate the cross section for a given process in a hadron-hadron collision one of the things we need to know are the parton distribution functions (PDF). In a proton, besides the constituent quarks $u\,u\,d$, there are virtual quark anti-quark pairs and gluons present. The probability distribution of these quarks know as partons (when quarks were yet to be discovered) at any instant determines the probability of an event of interest occurring during a collision and so it is important to know these distributions.

In the parton model a high energy proton or a hadron is regarded as a collection of

quasi-free partons. Thus in a proton, the momentum $P$ is considered to be a sum

$$\sum_i p_i = P$$

where $p_i = x_i P$ is the parton momentum and $x_i$ the fraction of the proton momentum carried by the parton.

Let $f_{a/A}(x_a)$ be the probability of finding parton $a$ in hadron $A$ with momentum $p_a = x_a P_A$ where $P_A$ is the momentum of hadron $A$. The cross section for producing a quark or a lepton $c$ and $d$ in the reaction

$$A + B \to c + d + \text{anything}$$

is obtained by multiplying the cross section $\hat{\sigma}$ for the process

$$a + b \to c + d + \text{anything}$$

by the probability density of the momentum fraction of the partons $a$ and $b$ and integrating over the momentum range that is kinematically accessible to these partons. The cross section for the process $A + B \to c + d + X$ can be written as [39]

$$\sigma(A + B \to c + d + X) = \int \mathrm{d}x_a \, \mathrm{d}x_b \left[ f_{a/A}(x_a) \, f_{b/B}(x_b) + (A \leftrightarrow B \text{ if } a \neq b) \right] \hat{\sigma}(a + b \to c + d + X).$$

The integration variables $x_a$ and $x_b$ can be written in terms of the invariant mass of the

partons $M_{ab}$ and the rapidity $y$ as

$$M_{ab}^2 = x_a x_b s$$

$$y = \frac{1}{2} \ln \frac{x_a}{x_b}$$

where $s = (P_A + P_B)^2$ and the masses of the partons and the protons have been neglected.

Rewriting the cross section we get

$$\sigma = \int_{M_{\text{min.}}}^{M_{\text{max.}}} \frac{2M}{s} \, \mathrm{d}M \int_{y_{\text{min.}}}^{y_{\text{max.}}} \mathrm{d}y \left[ f_{a/A}(x_a) \, f_{b/B}(x_b) + (A \leftrightarrow B \, \text{if} \, a \neq b) \right] \int_{-1}^{1} \frac{\mathrm{d}\hat{\sigma}(ab \to cd)}{\mathrm{d}z} \, \mathrm{d}z \int_{0}^{2\pi} \mathrm{d}\phi$$

where

$$y_{\text{max}} = \ln \frac{\sqrt{s}}{M_{ab}}$$

$$y_{\text{min}} = -y_{\text{max}}$$

$$z = \cos\theta$$

and $\theta$ and $\phi$ are the spherical coordinates in the center of mass frame of $a$ and $b$. $M_{\text{min}}$ is the minimum energy that $\sqrt{\hat{s}}$ can have which is the mass of $c$ and $d$ and the maximum energy $\hat{s}$ can take is the beam energy $\sqrt{s}$. This basic parton model has to be modified for our purposes. The most important modification is the change in the PDF due to QCD corrections. In leading logarithmic approximation [40] these corrections are independent of

the scattering process and can be accounted for by redefining the PDF as

$$f_{a/A}(x_a) \to f_{a/A}(x_a, Q^2)$$

where $Q^2$ is the scale factor which is usually taken to be $\hat{s}$. Although the scale factor is process independent it does affect the event rate and we shall see later that we choose $M_Z + M_A$ as our scale factor where $M_Z$ and $M_A$ are the $Z$ boson and the Higgs pseudoscalar masses.

Our process of interest is the bottom quark fusion from a $p\,p$ collision at the LHC which results in the production of a $Z$ boson and a pseudoscalar Higgs. The $Z$ boson decays into a lepton pair and the pseudoscalar decays into a bottom quark pair. The cross section for this process is

$$\begin{aligned}\sigma(p+p \to Z + A^0 + X) = \int_{M_Z+M_A}^{\sqrt{s}} \frac{2M}{s}\,\mathrm{d}M \int_{\frac{\ln\tau}{2}}^{\frac{-\ln\tau}{2}} \mathrm{d}y\, 2\,(BT1 \times BT2) \\ \times \int_{-1}^{1}\int_{0}^{2\pi} \frac{\mathrm{d}\hat{\sigma}(b\,\bar{b} \to Z A^0)}{\mathrm{d}z_1\,\mathrm{d}\phi_1}\,\mathrm{d}z_1\,\mathrm{d}\phi_1 \\ \times \int_{-1}^{1}\int_{0}^{2\pi} \frac{\Gamma(Z \to l\,\bar{l})}{\Gamma_Z}\,\mathrm{d}z_2\,\mathrm{d}\phi_2 \\ \times \int_{-1}^{1}\int_{0}^{2\pi} \frac{\Gamma(A^0 \to b\bar{b})}{\Gamma_{A^0}}\,\mathrm{d}z_3\,\mathrm{d}\phi_3\end{aligned}$$

where $BT1$ and $BT2$ are the PDFs for the bottom quarks and $\frac{\Gamma(Z \to l\bar{l})}{\Gamma_Z}$ is the branching fraction for the $Z$ decay to leptons and $\frac{\Gamma(A^0 \to b\bar{b})}{\Gamma_{A^0}}$ is the branching fraction for the decay

of $A^0$ to bottom quarks.

In two Higgs doublet models the Higgs scalar and pseudoscalar can be searched simultaneously through complimentary channels $A^0 \to Zh^0$ [18, 33, 37, 41] with a coupling proportional to $\cos(\beta - \alpha_H)$ and $H^0 \to ZA^0$ with coupling proportional to $\sin(\beta - \alpha_H)$. At the LHC the gluon fusion can be a significant source of a Higgs pseudoscalar through triangle and box diagrams with third generation quarks [42, 43]. For $\tan\beta \lesssim 10$, the top quark loop diagrams make a dominant contribution to the gluon fusion [42].

In the MSSM and a 2HDM in Model II Yukawa interactions [25], the model that was used in this study, one Higgs doublet couples to down-type quarks and charged leptons while another doublet couples to up-type quarks. The Higgs pseudoscalar does not couple with the gauge bosons and the $A^0 b\bar{b}$ coupling is proportional to $\tan\beta$ and therefore $A^0 \to b\bar{b}$ is the dominant decay channel for $\tan\beta \gtrsim 10$. The gluon fusion is a promising discovery channel to detect $pp \to ZA^0 \to l\bar{l}\,b\bar{b} + X$ via $g\,g \to ZA^0$ for $\tan\beta \sim 2$ and $m_A \lesssim 260$ GeV [44].

## 3.3 Production Cross Sections

The production cross section for $pp \to l\bar{l}\,b\bar{b} + X$ via $b\bar{b} \to ZA^0 \to l\bar{l}\,b\bar{b}$ is calculated in a 2HDM and the MSSM with Model II Yukawa interactions for the Higgs bosons and the fermions. The parton distribution functions of CTEQ6L1 [45] are used. The parton distribution functions are, as described in the previous section, the probability distribution of the fraction of the protons' momenta carried away by the partons which in this case are the bottom quark pairs. The production cross section of the bottom quark pairs and the

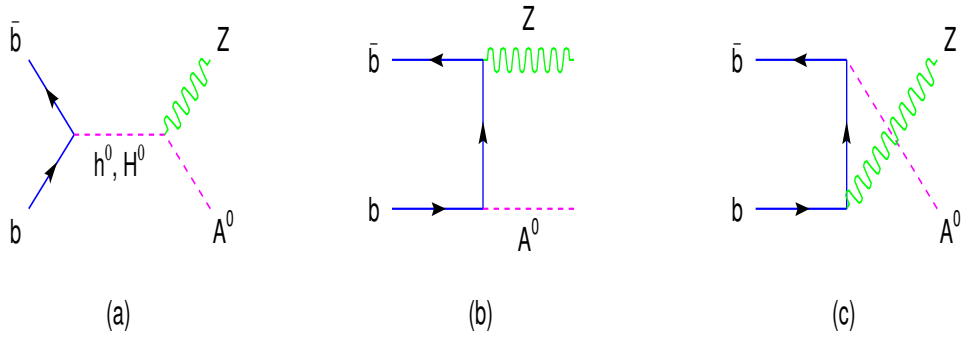


Figure 3.1: Feynman diagrams for the signal $b\bar{b} \to ZA^0$

lepton pairs that result from the Higgs decay and the $Z$ boson decay are calculated using the narrow width approximation. In the narrow width approximation the production cross section of $pp \to b\bar{b}\,l\,\bar{l} + X$ via $b\bar{b} \to ZA^0 \to l\,\bar{l}\,b\bar{b}$ is calculated by multiplying the cross section for $pp \to ZA^0$ by the branching fractions of $Z \to l\,\bar{l}$ and $A^0 \to b\,\bar{b}$.

In Figure 3.1 are the Feynman diagrams for $b\bar{b} \to ZA^0$ at the tree level . The $s$ channel diagrams contain the heavy Higgs scalar $H^0$ and light Higgs scalar $h^0$ in the intermediate state. This channel might provide a good opportunity to measure the couplings of $ZH^0A^0$ and $Zh^0A^0$. The $t$ and $u$ channels are proportional to $\tan\beta$ and when these channels dominate the cross section $b\bar{b} \to ZA^0$ is enhanced by $\tan^2\beta$. The unitarity condition that requires the total amplitude to disappear at very high energy was checked.

The cross section of $p\,p \to ZA^0 \to l\,\bar{l}\,b\,\bar{b} + X$ via $b\bar{b} \to ZA^0$ as a function of $\tan\beta$ are plotted in figure 3.2 for both the MSSM and a 2HDM. We have chosen $m_H = m_A + 100$ GeV, $m_h = 120$ GeV, and $\alpha_H = -\pi/4$ for a 2HDM. From the plot it can be seen that the cross section for a 2HDM is significantly larger than that for the MSSM when the heavy

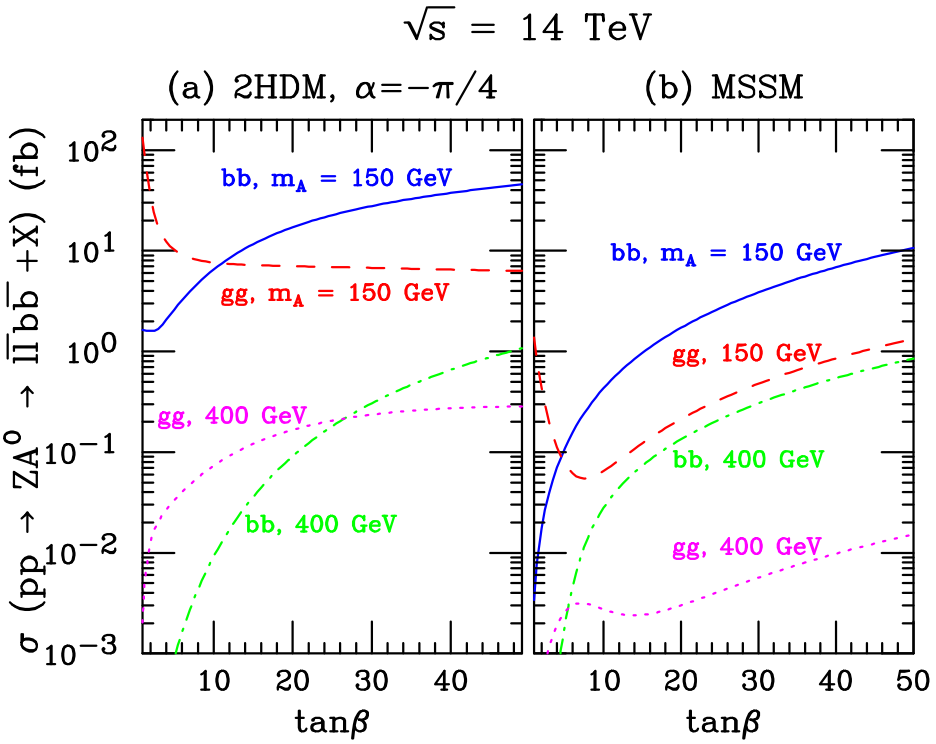


Figure 3.2: The cross section in fb without cuts for $p\,p \to Z A^0 + X \to l\,\bar{l}\,b\,\bar{b} + X$ at $\sqrt{s}$ = 14 TeV, as a function of $\tan\beta$, for $m_A$ = 150 and 400 GeV, in (a) a two Higgs doublet model with $m_h$ = 120 GeV, $m_H = m_A$ + 100 GeV and $\alpha_H = -\pi/4$ as well as in (b) the MSSM with $m_{\tilde{q}} = m_{\tilde{g}} = \mu$ = 1 TeV. We show contributions from bottom quark fusion ($b\,\bar{b} \to Z A^0$) and gluon fusion ($g\,g \to Z A^0$) separately.

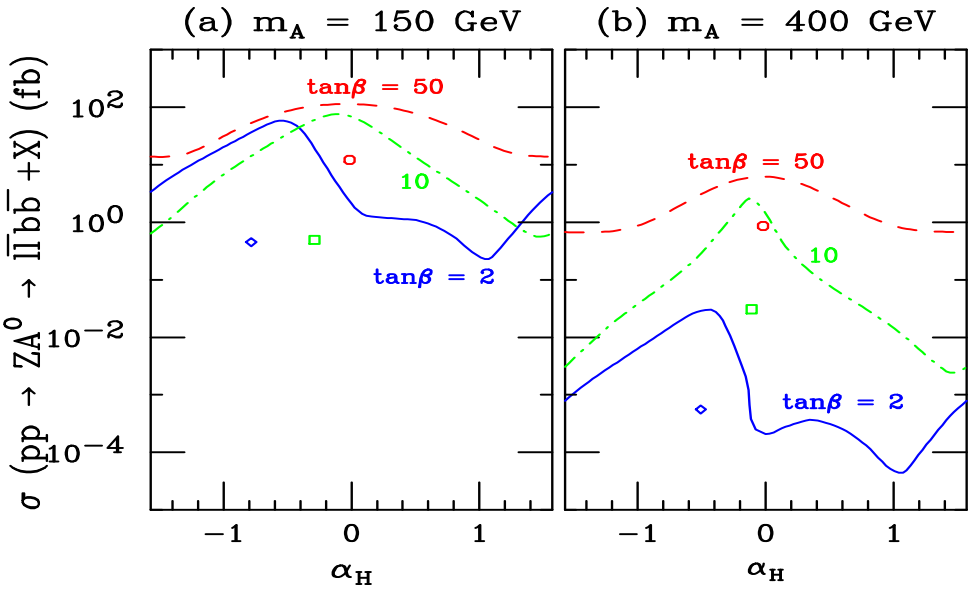


Figure 3.3: The cross section in fb without cuts for $pp \to ZA^0 + X \to l\,\bar{l}\,b\,\bar{b} + X$ at $\sqrt{s}$ = 14 TeV, as a function of the Higgs scalar mixing angle $\alpha_H$, in a 2HDM with $m_h$ = 120 GeV, $m_H = m_A + 100$ GeV with $\tan\beta$ = 2, 10 and 50, for (a) $m_A$ = 150 GeV and (b) $m_A$ = 400 GeV. Also shown are the cross sections in the MSSM for $\tan\beta$ = 2 (diamond), 10 (square), and 50 (circle). We include contributions from bottom quark fusion ($b\,\bar{b} \to ZA^0$) and gluon fusion ($g\,g \to ZA^0$).

Higgs scalar $H^0$ can decay into $ZA^0$. This is possible in a 2HDM because the mass of the heavy Higgs scalar and the mixing angle $\alpha_H$ are free parameters while they are fixed by the pseudoscalar mass $m_A$ and $\tan\beta$ in the MSSM. The mass of the heavy Higgs neutral scalar in the MSSM is given by

$$m_H^2 = \frac{1}{2}\left[m_A^2 + m_Z^2 + \sqrt{(m_A^2 + m_Z^2)^2 - 4m_Z^2 m_A^2 \cos^2 2\beta}\right].$$

Therefore $m_H$ is never greater or equal to $m_Z + m_A$ and so the decay $H^0 \to ZA^0$ is not kinematically accessible in the MSSM.

In figure 3.3 we show the effects of the Higgs scalar mixing angle ($\alpha_H$) on the cross section of $pp \to ZA^0 + X \to l\bar{l}b\bar{b} + X$ in 2HDM and MSSM for $m_A$ = 150 and 400 GeV

and $\tan\beta = 2$, 10, and 50. Both the bottom quark fusion ($b\bar{b} \to ZA^0$) and gluon fusion ($gg \to ZA^0$) are included in calculating the total cross section ($pp \to ZA^0 + X \to l\bar{l}b\bar{b} + X$).

For $m_A > m_Z + m_h$ and $m_A > m_t + m_W$ the Higgs pseudoscalar decay $A^0 \to b\bar{b}$ is suppressed by $A^0 \to Zh^0$ and $A^0 \to t\bar{t}^*$ with real and virtual top quarks. This explains why the cross section $pp \to ZA^0 \to l\bar{l}b\bar{b} + X$ is much greater for $m_A = 150$ GeV compared to $m_A = 400$ GeV.

## 3.4 Physics background

The programs MADGRAPH [46] and HELAS [47] were used to calculate the cross sections for all the physics backgrounds. The major contribution from the physics backgrounds to the final state $ZA^0 \to l\bar{l}b\bar{b}$ comes from $gg \to l\bar{l}b\bar{b}$, $q\bar{q} \to l\bar{l}b\bar{b}$, $l = e$ or $\mu$ and $q = u$, $d$, $s$, $b$ or $c$. The processes $gg \to bl^+\nu\bar{b}l^-\bar{\nu}$ and $q\bar{q} \to bl^+\nu\bar{b}l^-\bar{\nu}$ with dominant contribution from $pp \to t\bar{t} \to W^+W^-b\bar{b} + X$ was also calculated. We also considered the backgrounds from $pp \to l\bar{l}gb + X$, $pp \to l\bar{l}g\bar{b} + X$, $pp \to l\bar{l}gq + X$, $pp \to l\bar{l}g\bar{q} + X$, and $pp \to l\bar{l}jj + X$, where $j = g$, $q$ or $\bar{q}$ and $q = u$, $d$, $s$, or $c$.

For an integrated luminosity ($L$) of 30 fb$^{-1}$, we require two isolated leptons with transverse momentum $p_T(l) > 15$ GeV and pseudo rapidity $|\eta(l)| < 2.5$ in each event. The jets are required to have $p_T(b,j) > 15$ GeV and $|\eta(b,j)| < 2.5$. The $b$-tagging efficiency ($\epsilon_b$) is taken to be 60%; the probability of misidentifying a $c$- jet as a $b$- jet ($\epsilon_c$) is 10%, and the probability of mistagging any other jet ($\epsilon_j$) is 1%. To make sure the lepton pairs are from $Z$ decay we require the invariant mass of the lepton pair to be within 10 GeV of $M_Z$ which requires $|M_{l\bar{l}} - M_Z| \geq 10$ GeV.

The acceptance cuts are $p_T(l) > 25$ GeV and $p_T(b,j) > 30$ GeV for a higher integrated luminosity of 300 fb$^{-1}$. The $b$-tagging efficiency ($\epsilon_b$) is 50%, and $\epsilon_c$ is taken to be 14% while $\epsilon_j$ remains at 1%. These cuts remove most of the SM background while most leptons from the $Z$ decays and the Higgs decays have greater $p_T$ than these cuts thereby making it possible to detect them.

We require the missing transverse energy ($\not{E}$) in each event to be less than 20 GeV for $L$ = 30 fb$^{-1}$ and less than 40 GeV for $L$ = 300 fb$^{-1}$. This cut on missing energy along with the constraint on the invariant mass of the lepton pairs ($|M_{l\bar{l}} - M_Z| \leq 10$ GeV) effectively reduces the contribution from $pp \to W^+W^-b\bar{b} + X$ via $pp \to t\bar{t} + X$. These acceptance cuts and efficiencies of $b$- tagging and mistagging are similar to those of the ATLAS collaboration [37].

## 3.5 Discovery potential at the LHC

The background cross section from SM processes of $pp \to l\bar{l}b\bar{b} + X$ were calculated in the mass window $m_A \pm \Delta M_{b\bar{b}}$ where $\Delta M_{b\bar{b}} = 22$ GeV; $M_{b\bar{b}}$ is the invariant mass of the bottom quark pair from the ($A^0$) decay. The criterion we set for the Higgs signal [28, 48] to be observable if $\frac{N_S}{\sqrt{N_B}} > 5$ for a 5 $\sigma$ event and $\frac{N_S}{\sqrt{N_B}} > 3$ for a 3 $\sigma$ event; $N_S = \sigma_S \times L$ and $N_B$ = $\sigma_B \times L$; $\sigma_S$ and $\sigma_B$ correspond to the total cross section for the signal and background calculated within a bin of width $\pm\Delta M_{b\bar{b}}$ centered at $m_A$; $L$ is the integrated luminosity.

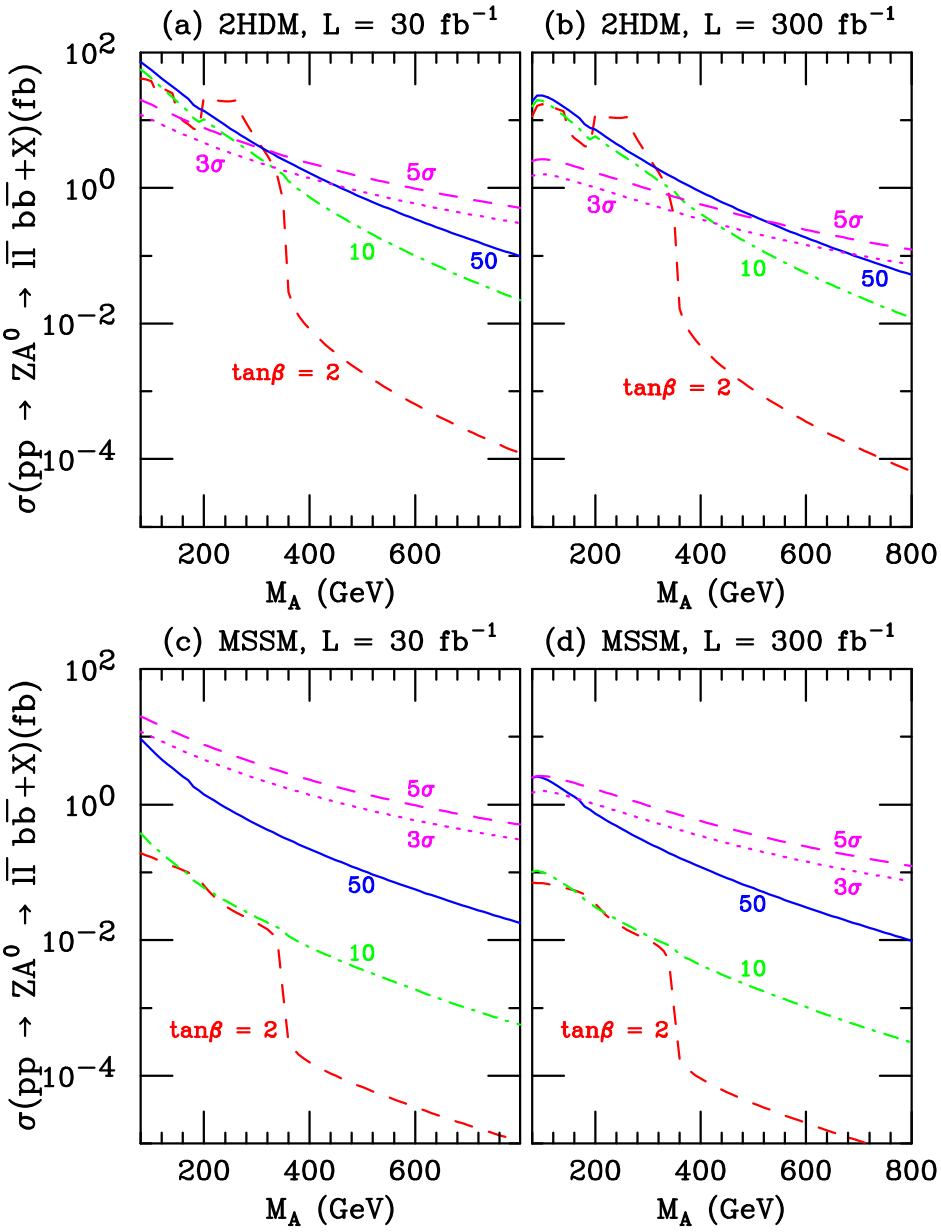


Figure 3.4: The cross section in fb for $pp \to ZA^0 + X \to l\bar{l}b\bar{b} + X$ versus $m_A$ at $\sqrt{s} = 14$ TeV, in a two Higgs doublet model with $m_h = 120$ GeV, $m_H = m_A + 100$ GeV and the Higgs scalar mixing angle $\alpha_H = \beta - \pi/2$, for $\tan\beta = 2$ (dashed), 10 (dot-dashed) and 50 (solid). The $5\sigma$ (dashed) and $3\sigma$ (dotted) cross sections for the $ZA^0$ signal required for an integrated luminosity ($L$) of (a) 30 fb$^{-1}$ and (b) 300 fb$^{-1}$ are also shown. The acceptance cuts, tagging and mistagging efficiencies have been applied as described in the text.

As described in the previous chapter the neutral Higgs coupling to the gauge bosons are

$$\frac{g_{hVV}}{g_{SM}} = \sin(\beta - \alpha_H)$$
$$\frac{g_{HVV}}{g_{SM}} = \cos(\beta - \alpha_H)$$

where $V = W$ or $Z$. For $\beta - \alpha_H = \pi/2$ the light Higgs coupling becomes identical to the SM coupling and the Heavy Higgs coupling dissppears. This is known as the decoupling limit [49]. In figure 3.4 we show the cross section $\sigma$ ($pp \to ZA^0 \to l\bar{l}b\bar{b} + X$) as a function of $m_A$ in a 2HDM for an integrated luminosity $L$ = 30 and 300 fb$^{-1}$; $\tan\beta$ = 2, 10, and 50; $m_H = m_A$ + 100 GeV, $m_h$ = 120 GeV, and the decoupling limit $\alpha_H = \beta - \pi/2$. In the MSSM only $\tan\beta$ and $m_A$ are the free parameters; figure 3.4 shows $\sigma$ ($pp \to ZA^0 \to l\bar{l}b\bar{b} + X$) as a function of $m_A$ with acceptance cuts for $\tan\beta$ = 2, 10, and 50; $L$ = 30 fb$^{-1}$ and 300 fb$^{-1}$. The $5\sigma$ and $3\sigma$ curves for the $ZA^0$ signal cross section are also presented. Both bottom quark fusion and gluon fusion contributions are included. In a 2HDM it is possible to establish a $5\sigma$ signal of $ZA^0 \to l\bar{l}b\bar{b}$ for $m_A \lesssim$ 200 GeV and $\tan\beta \sim 2$ or $\tan\beta \sim 50$ for an integrated luminosity of 30 fb$^{-1}$. For an integrated luminosity of 300 fb$^{-1}$ the discovery potential is greatly improved for $m_A \lesssim$ 280 GeV and $\tan\beta \sim 2$ or $\tan\beta \sim 50$. In the MSSM, the production cross section is small because $m_H \sim m_A$ which makes the decay $H^0 \to ZA^0$ kinematically inaccessible. In both 2HDM and MSSM the branching fraction of $A^0 \to b\bar{b}$ is greatly suppressed when the Higgs pseudoscalar decays dominantly into $Zh^0$ and $t\bar{t}^*$ with one of the top quarks ($t^*$) being virtual.

The table 3.1 gives the event rates after acceptance cuts for the Higgs signal ($N_S$) from $b\bar{b} \to ZA^0 \to l\bar{l}b\bar{b}$ in a 2HDM with $\tan\beta$ = 10 and 50 and $\alpha_H = -\pi/4$; the background

| $\tan\beta = 10$ | | | | |
|---|---|---|---|---|
| $m_A$ (GeV) | $N_S$ | $N_B$ | $N_S/N_B$ | $N_S/\sqrt{N_B}$ |
| 100 | 196 | $1.01 \times 10^4$ | 0.019 | 1.95 |
| 200 | 14 | 2100 | 0.007 | 0.30 |
| 300 | 1 | 577 | 0.001 | 0.03 |
| 400 | $< 1$ | 193 | $< 0.001$ | $< 0.01$ |
| $\tan\beta = 50$ | | | | |
| $m_A$ (GeV) | $N_S$ | $N_B$ | $N_S/N_B$ | $N_S/\sqrt{N_B}$ |
| 100 | 773 | $1.01 \times 10^4$ | 0.076 | 7.7 |
| 200 | 138 | 2100 | 0.066 | 3.0 |
| 300 | 31 | 577 | 0.054 | 1.3 |
| 400 | 9 | 193 | 0.045 | 0.62 |

Table 3.1: Event rates after acceptance cuts for the Higgs signal ($N_S = \sigma_S \times L$) from $b\bar{b} \to ZA^0$ and the background ($N_B = \sigma_B \times L$) as well as the ratio of signal to background $N_S/N_B$ and $N_S/\sqrt{N_B}$ in a two Higgs doublet model with $\tan\beta = 10$ and 50, $\alpha_H = -\pi/4$, and $m_H = m_A + 100$ GeV for an integrated luminosity of 30 fb$^{-1}$.

event rate ($N_B$) as well as the ratios $N_S/N_B$ and $N_S/\sqrt{N_B}$ are also presented. Figures 3.5 and 3.6 give the discovery contours for the $A^0$ signal via the bottom quark fusion at the LHC with the acceptance cuts, tagging and mistagging efficiencies having been applied. The curve for the decoupling limit $\beta - \alpha_H = \pi/2$ is also presented. For $L = 30$ fb$^{-1}$ the parameter space $|\alpha_H| \lesssim 0.5$ and $m_A \lesssim 250$ GeV is a promising discovery channel and for $L$ = 300 fb$^{-1}$ the discovery potential is greatly improved for $|\alpha_H| \lesssim 1$ and $m_A$ up to 400 GeV. The discovery potential of $A^0$ with $Z$ boson at the LHC through a bottom quark fusion and gluon fusion are found to be complementary. The bottom quark fusion can make dominant contributions to the production of $A^0$ with Z boson at the LHC for $\tan\beta \gtrsim 10$ while the gluon fusion is the major source for $\tan\beta \lesssim 10$.

| $\tan\beta = 10$ | | | | |
|---|---|---|---|---|
| $m_A$ (GeV) | $N_S$ | $N_B$ | $N_S/N_B$ | $N_S/\sqrt{N_B}$ |
| 100 | 897 | $2.62 \times 10^4$ | 0.034 | 5.5 |
| 200 | 75 | $1.02 \times 10^4$ | 0.007 | 0.74 |
| 300 | 4 | 3380 | 0.001 | 0.06 |
| 400 | $< 1$ | 1170 | $< 0.001$ | 0.01 |
| $\tan\beta = 50$ | | | | |
| $m_A$ (GeV) | $N_S$ | $N_B$ | $N_S/N_B$ | $N_S/\sqrt{N_B}$ |
| 100 | 3310 | $2.62 \times 10^4$ | 0.13 | 20.5 |
| 200 | 731 | $1.02 \times 10^4$ | 0.07 | 7.2 |
| 300 | 168 | 3380 | 0.05 | 2.9 |
| 400 | 46 | 1170 | 0.04 | 1.4 |

Table 3.2: The same as in 3.1, except that the integrated luminosity is 300 fb$^{-1}$.

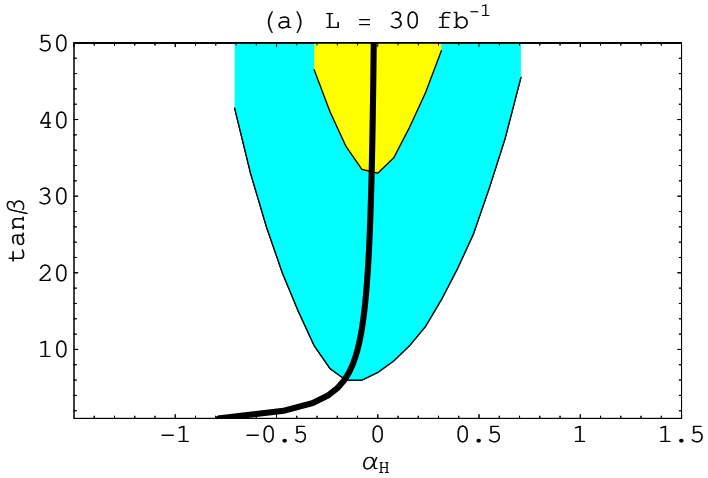


Figure 3.5: The $5\sigma$ discovery contours at the LHC with an integrated luminosity ($L$) of 30 fb$^{-1}$ in the ($\alpha_H$, $\tan\beta$) plane for $m_A = 150$ GeV (medium shading), $m_A = 250$ GeV (light shading)in a two Higgs model with $m_h = 120$ GeV and $m_H = m_A + 100$ GeV. The discovery region is the parameter space above the contours. The curve represents the decoupling limit $\beta - \alpha_H = \pi/2$. The Higgs signal is from $b\bar{b} \to ZA^0$ alone. The acceptance cuts, tagging and mistagging have been applied as described in the text.

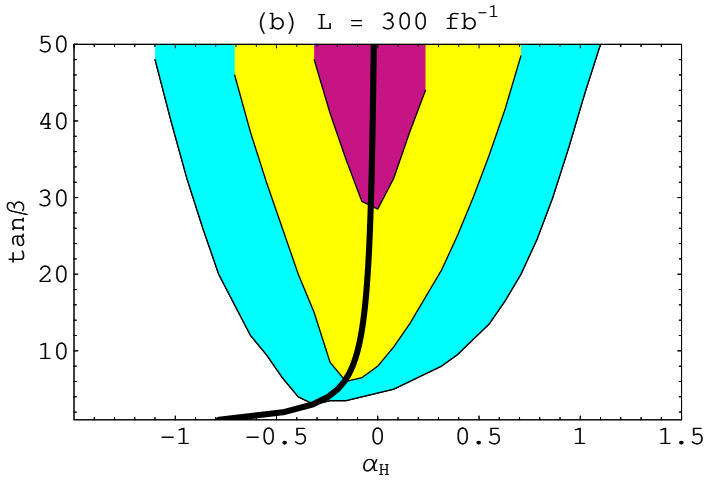


Figure 3.6: Same as 3.5 except the dark shading is for 400 GeV.

In 2HDM the results are promising for $pp \to ZA^0 \to l\bar{l}b\bar{b} + X$ via $b\bar{b} \to ZA^0$ at the LHC with $L = 300\text{fb}^{-1}$ for $m_A \lesssim 400\text{GeV}$, $\tan\beta \gtrsim 5$, $|\alpha_H| \lesssim 1$ and $m_H = m_A + 100$ GeV. The production cross section is small in the MSSM because $m_A \sim m_H$ making the decay $H^0 \to ZA^0$ kinematically inaccessible.

For $m_A \lesssim 260\text{GeV}$ and $\tan\beta \sim 2$ the gluon fusion contribution to the production of $ZA^0$ is dominant [44]. The gluon contribution is reduced especially when $\tan\beta \sim 7$ due to the destructive interference between the triangle and box diagrams as well as negative interference between the top quark and bottom quark loops [42].

## 3.6 Summary

In 2HDM the discovery potential of a Higgs pseudoscalar through $b\bar{b} \to ZA^0$ and the gluon fusion ($gg \to ZA^0$) can be greatly enhanced when the heavier neutral scalar Higgs ($H^0$) can decay into the Higgs pseudoscalar and a $Z$ boson. The Higgs production cross section in 2HDM reduces to MSSM levels when $m_H \sim m_A$. Therefore if the heavier Higgs ($H^0$)

can decay into a $Z$ boson and a Higgs pseudoscalar it might provide a good opportunity to discover simultaneously both the heavy neutral Higgs scalar and the pseudoscalar.

# Chapter 4

# Detecting Higgs Bosons with Bottom Quarks

## 4.1 Introduction

In this chapter we discuss the discovery potential at the LHC of a neutral Higgs in the MSSM. The discovery channel studied is the bottom gluon fusion and detecting the bottom quark pair produced from the Higgs decay. The bottom quark Higgs couplings are enhanced by factors of $1/\cos\beta$ in the Model II of two Higgs doublet models [25] which is the model used in this study. In MSSM there are only two free parameters and as before we choose $m_A$ and $\tan\beta$ as the two free parameters.

## 4.2 Production Cross Section

The production cross section for the process $pp \to b\phi^0 + X \to bb\bar{b} + X$ via $bg \to b\phi^0$ is calculated by multiplying the Higgs signal cross section $bg \to b\phi^0$ with the branching fraction of the Higgs decay to a bottom quark pair. The production cross section also includes the Higgs resulting from anti-bottom gluon fusion and $b$ quark shall denote both bottom and anti-bottom quarks for the rest of the chapter unless otherwise specified. The neutral Higgs $\phi^0$ refers to the light and heavy scalars ($h^0$ and $H^0$) and the pseudoscalar ($A^0$). The cross section was calculated in the MSSM with Model II Yukawa interactions for the Higgs bosons and fermions. The parton distribution functions CTEQ6L1 [45] were used to calculate the probability distribution of the initial bottom quark and the gluon.

For $m_A < 125$ GeV the total cross section is from the pseudoscalar Higgs $A^0$ and the lighter Higgs $h^0$ because $m_A \sim m_h$ in this mass range. The total cross section for $m_A > 125$ GeV is the sum of the cross sections for $A^0$ and the heavier Higgs $H^0$.

The cross section as a function of the transverse momentum of the bottom quarks is shown in figure 4.1 for $m_A = 200$ and 400 GeV and $\tan\beta = 10$ and 50. The enhancement in the signal as $\tan\beta$ increases can be seen in figure 4.1. The enhancement is due to the $A^0\, b\,\bar{b}$ coupling being proportional to $\tan\beta$ which results in the cross section being proportional to $\tan^2\beta$. A similar enhancement is seen in the figure 4.2 where the cross section is plotted as a function of the invariant mass for the same parameters as figure 4.1. In figure 4.2 $M_{12}$, $M_{13}$, and $M_{23}$ refer to the invariant mass of the most energetic bottom quark pairs to the least energetic. Gaussian smearing has been used to smooth the peaks in the plots.

## 4.3 SM Background

The dominant physics background to the final state of $b\,b\,\bar{b}$ come from $b\,g \to b\,b\,\bar{b}$, $c\,g \to c\,b\,\bar{b}$, and $q\,g \to q\,b\,\bar{b}$ where $q = u$, $d$, and $s$. There is also background contribution from $q\,\bar{q} \to g\,b\,\bar{b}$ where $q = u$, $d$, $b$, $s$, and $c$. The contribution due to the anti-quarks were also calculated. For an integrated luminosity ($L$) of 30 fb$^{-1}$ we require the two most energetic jets of the three jets to have transverse momentum $p_T > 25$ GeV and the third jet to have $p_T > 15$ GeV. All three jets also should have the absolute value of pseudo-rapidity $|\eta|$ to be less than 2.5. MADGRAPH [46] and HELAS [47] were used to calculate the cross sections for all the SM background and the parton distribution functions of CTEQ6L1 [45] were used to calculate the parton momentum.

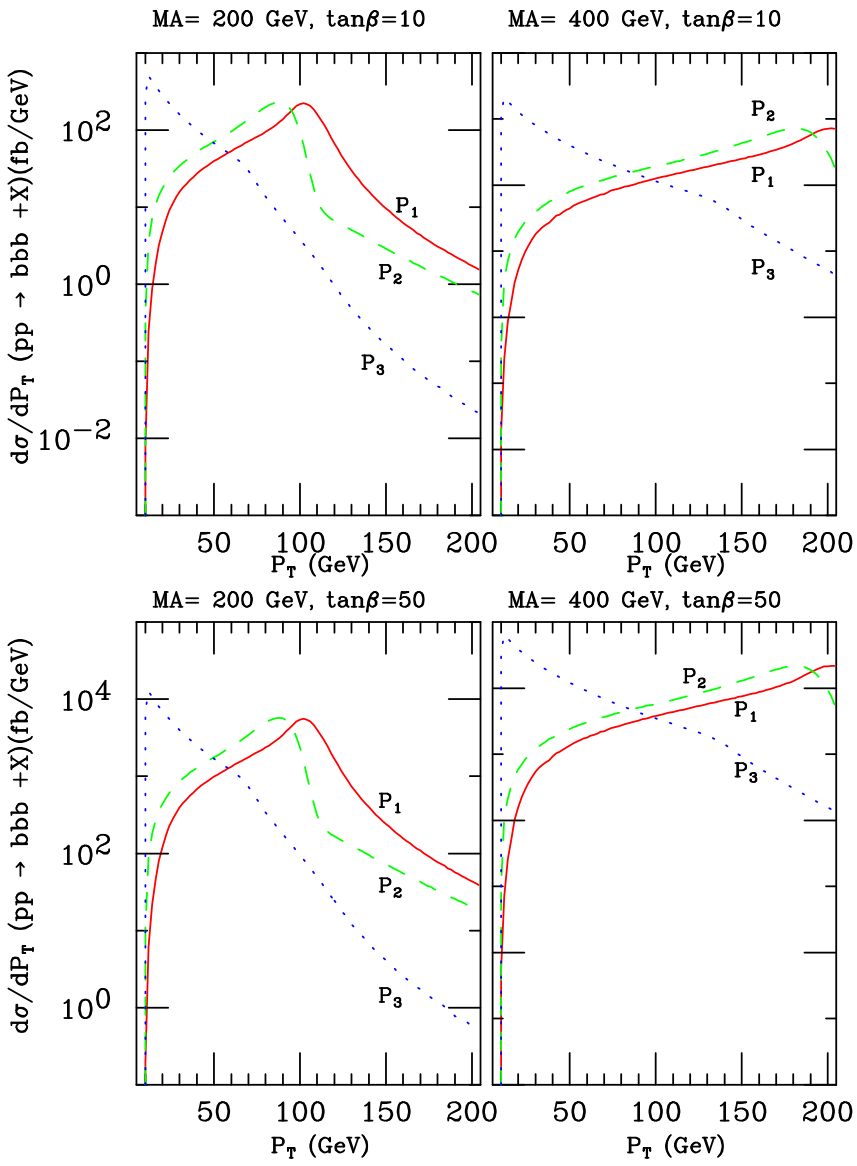


Figure 4.1: The transverse momentum ($P_T$) distributions in fb/GeV for the bottom quarks in $pp \to b\,g \to b\,A \to b\,b\bar{b}$ at $\sqrt{s} = 14$ TeV for $m_A = 200$ and 400 GeV and $\tan\beta = 10$ and 50.

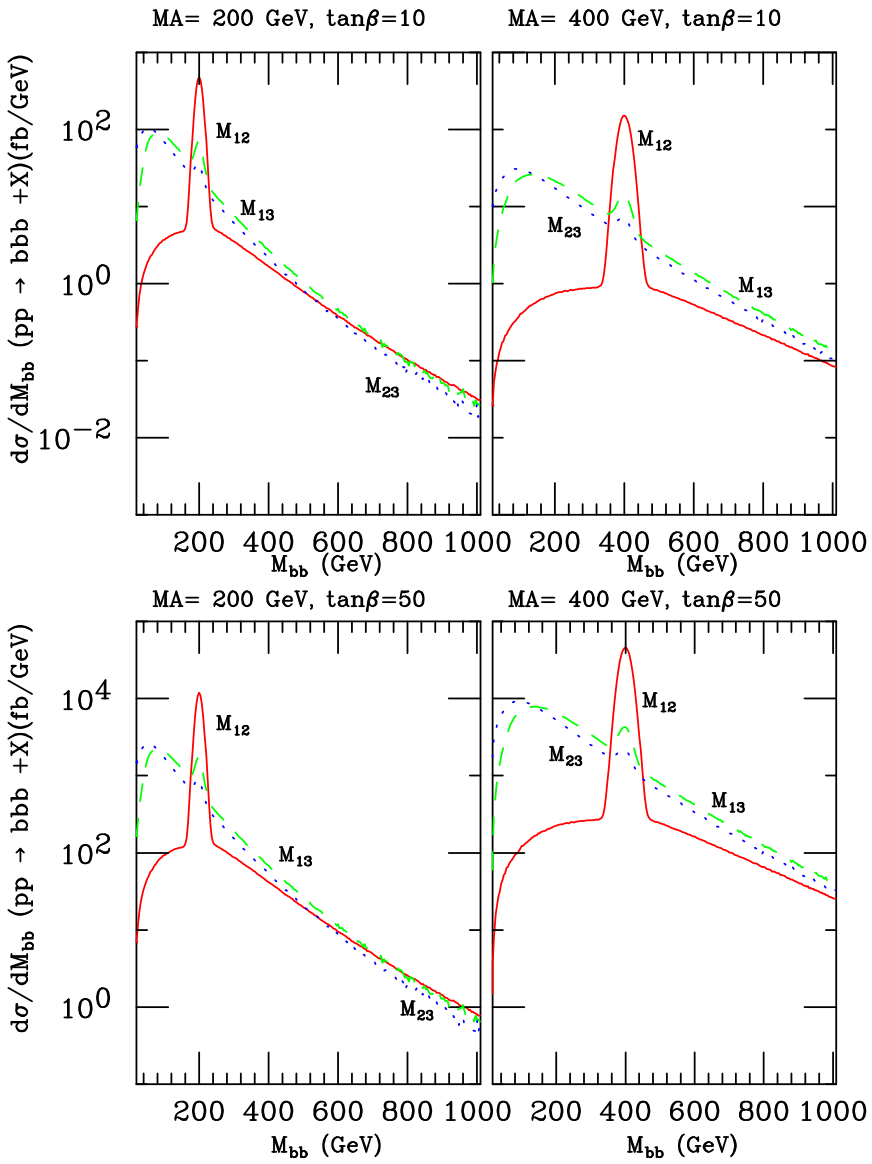


Figure 4.2: The invariant mass distributions in fb/GeV for the bottom quarks in $pp \to b\,g \to b\,A \to b\,b\bar{b}$ at $\sqrt{s} = 14$ TeV for the same parameters as fig. 4.1.

The contribution due to $q\,\bar{q} \to b\,\bar{b}\,j\,j$ where $q = b$, $u$, $d$, $s$, $c$ and $j = u$, $d$, $s$, $c$, $g$ were also calculated. For an integrated luminosity of 30 fb$^{-1}$ events with all four jets with $p_T >$ 15 GeV and $|\eta| < 2.5$ were vetoed and only the events with two jets having $p_T > 25$ GeV and a third jet with $p_T > 15$ GeV and all three with $|\eta| < 2.5$ were accepted.

The background from $g\,g \to b\,\bar{l}\,\nu\,\bar{b}\,\bar{u}\,d$ and $g\,g \to b\,\bar{d}\,u\,\bar{b}\,\bar{u}\,d$ with dominant contribution from $p\,p \to t\,\bar{t} \to b\,W^+\,\bar{b}\,W^- + X$ were also evaluated. The $l$ are the electrons and the muons and $\nu$ are their corresponding neutrinos. The $u$ and $d$ are the up-type and down-type quarks with the exception of the top and bottom quarks. For an integrated luminosity of 30 fb$^{-1}$ we vetoed events with all four jets or at least four jets in the six jet case with $p_T$ $> 15$ GeV and $|\eta| < 2.5$. Also for the $b\,\bar{l}\,\nu\,\bar{b}\,\bar{u}\,d$ final state we require for the lepton to have $p_T < 20$ GeV or the missing energy $\not{E}$ due to the neutrino to be to be less than 20 GeV. The same acceptance cuts were used for $L = 300$ fb$^{-1}$, but for the two most energetic jets the acceptance cut is $p_T > 30$ GeV for all the background.

As in the previous chapter the tagging efficiency $\epsilon_b$ for a $b$ jet is taken to be 60% and the possibility of identifying a $c$ jet to be a $b$ jet is taken to be $\epsilon_c = 10\%$. The probability of misidentifying all other jets as a $b$ jet is taken to be $\epsilon_j = 1\%$ for $L = 30$ fb$^{-1}$. For $L =$ 300 fb$^{-1}$: $\epsilon_b = 50\%$, $\epsilon_c = 10\%$, and $\epsilon_j = 1\%$.

## 4.4 Discovery Potential at the LHC

The background cross section from only $b\,g \to b\,b\,\bar{b}$, $c\,g \to c\,b\,\bar{b}$, $q\,g \to b\,b\,\bar{b}$ where $q = u$, $d$, and $s$; $b\,\bar{b} \to g\,b\,\bar{b}$ and $q\,\bar{q} \to g\,b\,\bar{b}$ where $q = u$, $d$, $c$, and $s$; $q\,\bar{q} \to b\,\bar{b}\,j\,j$ where $q = u$, $d$, $s$ and $c$ and $j = u$, $d$, $s$, and $b$. are presented here. The background event was accepted if

the invariant mass of at least one bottom quark lies within a mass window of $m_A \pm \Delta\, M_{bb}$ where $\Delta\, M_{bb} = 22$ GeV. The criterion used for the Higgs signal to be observable [28, 48] is the same as in the previous chapter which is $\frac{N_S}{\sqrt{N_B}} > 5$ for a 5 $\sigma$ event and $\frac{N_S}{\sqrt{N_B}} > 3$ for a 3 $\sigma$ event; $N_S = \sigma_S \times L$ and $N_B = \sigma_B \times L$; $\sigma_S$ and $\sigma_B$ correspond to the total cross section for the signal and background calculated within a bin of width $\pm\Delta M_{bb}$ centered at $m_A$.

Figure 4.3 shows the total signal cross section vs $m_A$ for $\tan\beta = 2$, 10, and 50. Figure 4.4 presents the discovery contour at an integrated low luminosity of $L = 30$ fb$^{-1}$ in the $m_A - \tan\beta$ plane.

## 4.5 Summary

The discovery potential of a neutral Higgs in a bottom quark gluon fusion looks promising for $\tan\beta > 10$. For smaller values of $\tan\beta$ the production cross section is small to be detected over the background. Although the branching ratio for $\phi^0 \rightarrow b\,\bar{b}$ is larger than that for $\phi^0 \rightarrow \tau^+\,\tau^-$ and $\phi^0 \rightarrow \mu^+\,\mu^-$, smaller physics background makes the tau pair and the muon pair discovery channels more significant than the bottom quark pair [36, 50, 51].

In addition, we note that the discovery channel with one bottom quark in the final state ($b\,\mu^+\,\mu^-$, $b\,\tau^+\,\tau^-$, $b\,b\,\bar{b}$) is more promising than the inclusive processes $\phi^0 \rightarrow \mu^+\,\mu^-$, $\tau^+\,\tau^-$, and $b\,\bar{b}$ and the associate production of bottom quark pairs ($\phi^0\,b\,\bar{b} \rightarrow \mu^+\,\mu^-\,b\,\bar{b}$, $\tau^+\,\tau^-\,\mu^+\,\mu^-$, and $b\,\bar{b}\,b\,\bar{b}$) [36, 52]. The discovery of $\phi^0 \rightarrow \mu^+\,\mu^-$, $\tau^+\,\tau^-$, and $b\,\bar{b}$ decays will provide an excellent opportunity to study the Yukawa couplings of the Higgs bosons with the fermions.

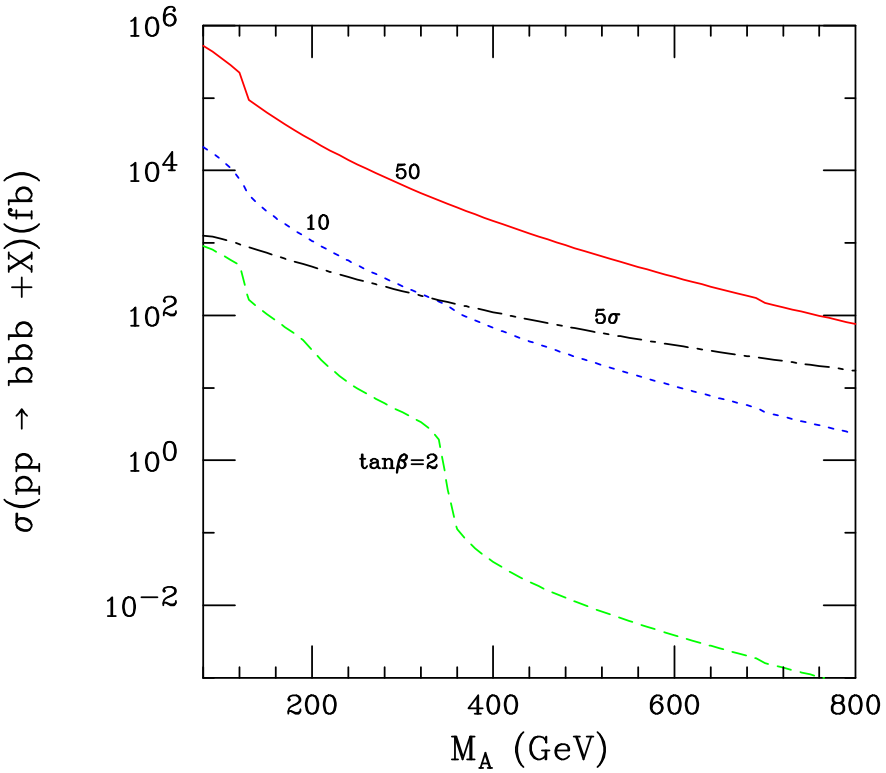


Figure 4.3: The cross section in fb for $p\,p \rightarrow b\,\phi^0 + X \rightarrow b\,b\,\bar{b} + X$ for an integrated luminosity $L = 30$ fb$^{-1}$. The parameter space above the $5\sigma$ line represents the observable Higgs signal. The background cross section is from the processes $q\,g \rightarrow q\,b\,\bar{b}$, $q\,\bar{q} \rightarrow g\,b\,\bar{b}$, and $q\,\bar{q} \rightarrow b\,\bar{b}\,j\,j$ where $q = b$, $u$, $d$, $s$, $c$ and $j = u$, $d$, $s$, $c$, $g$. The acceptance cuts, tagging, and mistagging efficiencies described in text have been applied.

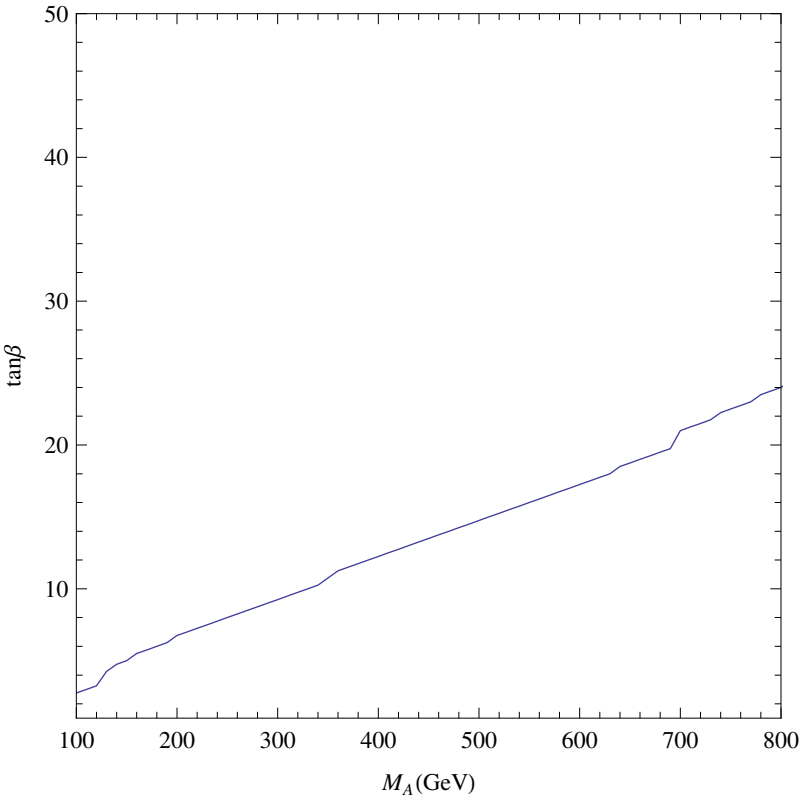


Figure 4.4: The $5\sigma$ discovery contour at the LHC for an integrated luminosity of 30 fb$^{-1}$ in the $M_A - \tan\beta$ plane. The signal includes $\phi^0 = A^0$ and $h^0$ for $M_A < 125$ GeV and $\phi^0 = A^0$ and $H^0$ for $M_A \geq 125$ GeV. The discovery region is the parameter space above the contour. The acceptance cuts, tagging, and mistagging efficiencies described in text have been applied.

# Chapter 5

# Discovery Potential at the Large Hadron Collider

At the LHC it will be possible to detect the SM Higgs boson from the lower limit of 114.4 GeV set by the four LEP experiments [9] to the TeV scale after running for a few years. In general two Higgs doublet models (2HDMs) there are five physical bosons, which are the two neutral $CP$-even scalars $h^0$ and $H^0$, one $CP$-odd pseudoscalar $A^0$, and the two charged Higgs $H^{\pm}$. In a $CP$ conserving 2HDM, there are six free parameters: the four Higgs masses, the ratio of the vacuum expectation values $\tan\beta$, and the mixing angle $\alpha$. At the tree level, in the MSSM, all Higgs boson masses and couplings can be calculated from two free parameters usually chosen to be the pseudoscalar Higgs boson mass ($m_A$) and $\tan\beta$. At the LHC the entire region of the parameter space $m_A$ = 50-1000 GeV and $\tan\beta$ = 1-50 should be accessible for the discovery of at least one Higgs boson of minimal supersymmetry [17, 18].

## 5.1 SM Higgs searches

At the LHC the SM Higgs is searched for in various decay channels: $H \to \gamma\gamma$, $H \to b\bar{b}$, $H \to ZZ^* \to 4l$, $H \to ZZ \to lljj$, $H \to ZZ \to ll\nu\nu$, and $H \to WW \to l\nu jj$. The discovery potential of the various decay channels depends on the signal rate and the signal to background ratio.

The decay $H \to \gamma\gamma$ is a rare decay mode and is only observable when the production cross-section and the decay branching ratio are both reasonably large. The production

cross-section of a low-mass Higgs boson (80 GeV $\lesssim m_H \lesssim$ 150 GeV) is dominated by gluon fusion and the decay $H \rightarrow \gamma\,\gamma$ is a promising discovery channel in this mass region due to the relatively small physics background.

If the SM Higgs boson is lighter than 140 GeV the decay $H \rightarrow b\bar{b}$ is dominant with a branching ratio of $\sim$ 90%. This decay channel is important for both the discovery of the Higgs particle and to measure the Higgs coupling to bottom quarks. The associated production of a Higgs with a $W$ or a $Z$ boson or a top quark pair are possible discovery channels to observe the Higgs decay into a bottom quark pair.

In the mass range $\gtrsim$ 130 GeV to 2 $m_Z$ the decay channel $H \rightarrow W\,W^*\,l\,\nu\,\nu$ and $H \rightarrow Z\,Z^* \rightarrow 4l$ provide clean signatures. For the Higgs boson mass in the range 180 GeV $< m_H \lesssim$ 700 GeV the gold plated channel $Z\,Z \rightarrow 4l$ is the most reliable channel for the discovery of the SM Higgs at the LHC and is used for the precise reconstruction of the Higgs mass. In the mass range 300 GeV to 1 TeV the SM Higgs can be detected through the decay channels $H \rightarrow Z\,Z \rightarrow l\,l\,\nu\,\nu$, $H \rightarrow W\,W \rightarrow l\,\nu\,j\,j$, and $H \rightarrow Z\,Z \rightarrow l\,l\,j\,j$.

Figure 5.1 shows at least two discovery channels available over most of the Higgs mass range [17, 37]. The comparison of production rates between the various decay channels will provide important information for determining the SM Higgs mass, width, production rates, and branching ratios.

## 5.2 The search for the MSSM Higgs

The search for the MSSM Higgs bosons has to begin with the search for the lightest Higgs scalar. Since the neutral scalars were the focus of this study we will focus only on the

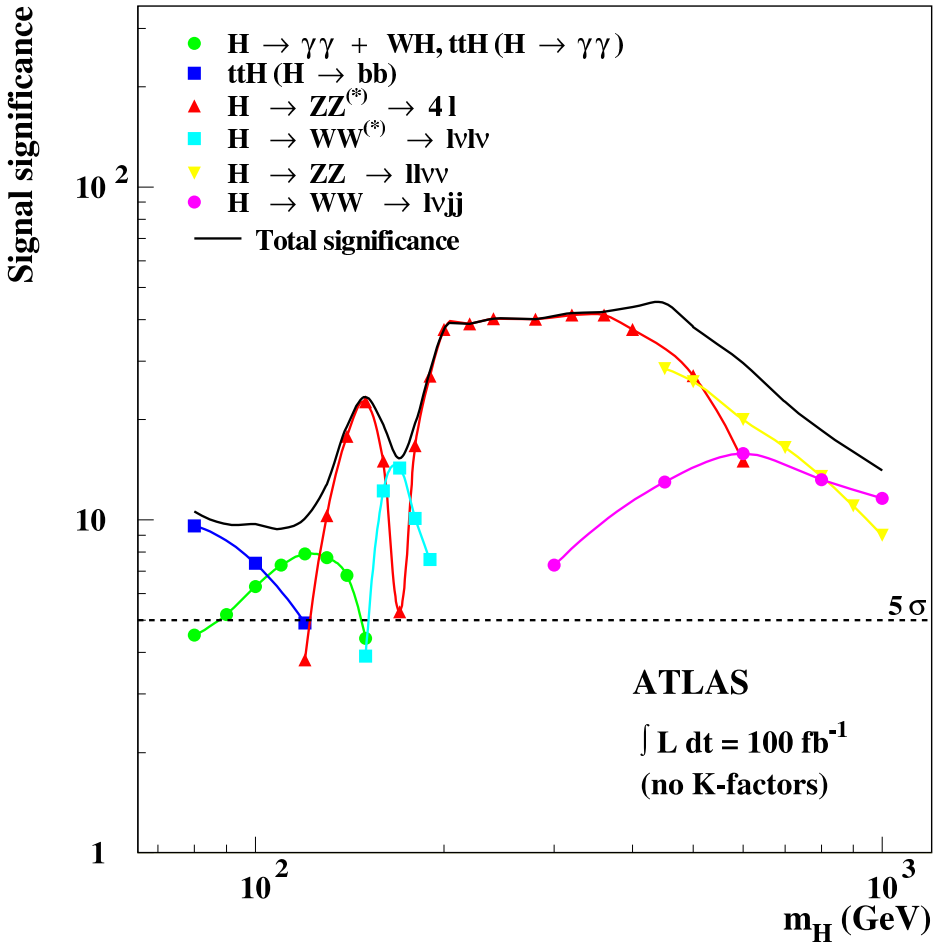


Figure 5.1: The sensitivity of the ATLAS detector to the discovery of the SM Higgs through various channels. The significance is the ratio $S/\sqrt{B}$ where $S$ is the number of signal events and $B$ is the number of background events [37]. All calculations do not include radiative corrections (no K-factors).

neutral Higgs bosons. In the $CP$ conserving model studied in this thesis the lightest Higgs is the neutral $CP$-even neutral scalar $h^0$. In the decoupling limit ($\tan\beta \gtrsim$, $m_A \gg m_Z$, $\cos(\beta-\alpha) \to 0$) $h^0$ resembles the SM Higgs and all the search techniques used for the SM Higgs apply. For a fixed $\tan\beta$ and $m_A \gg m_Z$ the tree level value of $m_h$ is maximum and is $m_h^{max.} = m_Z$ and when radiative corrections are included the maximum value increases to 135 GeV. For values of $m_A < m_h^{max.}$ and large $\tan\beta$ the heavy neutral $CP$-even scalar $H^0$ resembles the SM Higgs.

The decay channel $\phi^0 \to \gamma\,\gamma$ where $\phi^0 = h^0$, $H^0$ can be used to detect $h^0$ and $H^0$. when $\phi^0$ is produced either by the direct production through gluon or vector boson fusion or produced in association with $W^\pm$ or $t\,\bar{t}$ production. The $h^0 \to b\,\bar{b}$ can be observed when $h^0$ is produced in association with $t\,\bar{t}$. The $\phi^0 \to \gamma\,\gamma$ and $h^0 \to b\,\bar{b}$ decay channel are complimentary and cover most of the $m_A$-$\tan\beta$ plane.

The $H^0 \to \tau\,\tau$ decay mode is strongly enhanced compared to the SM Higgs boson because it is very difficult to observe the SM signal over the large background. For low values of $\tan\beta$, and $m_A \leq m_t$, the direct production of $A^0$ through gluon fusion and the $A^0 \to \tau\,\tau$ decay mode are dominant and significantly larger than the SM Higgs of same mass. For large values of $\tan\beta$ the associated production of Higgs bosons with bottom quarks dominate. For $m_A > 150$ GeV the $H^0$ and $A^0$ masses are degenerate and can be summed. The $H^0 + A^0 \to \tau\,\tau$ branching ratio is 10% in the mass range $m_A = 200$-$500$ GeV and the relative contribution from the associated production $b\,\bar{b}\,H^0$ and $b\,\bar{b}\,A^0$ is about 50% for $\tan\beta = 5$ and around 90% for $\tan\beta = 20$ [37].

As in the case of $H^0 \to \tau\,\tau$ the SM Higgs signal in the $H^0 \to \mu\,\mu$ decay cannot be observed at the LHC due to both the weak signal rate and the large background. In the

MSSM the $H^0$ and $A^0$ signal can be observed at $\tan\beta > 10$ and the light Higgs $h^0$ should be observable in the region $m_A \lesssim 125$ GeV and $\tan\beta > 5$ [35]. The $\mu\,\mu$ channel can be used for the precise reconstruction of the Higgs mass.

In the MSSM $m_A \simeq m_H$ making it difficult to detect the pseudoscalar Higgs $A^0$ with a $Z$ boson. In a general two Higgs doublet model, it is possible to detect the $A^0$ in $H^0$ decays at the LHC for a high integrated luminosity of $L = 300$ fb$^{-1}$, $m_A \lesssim 260$ GeV, $m_H = m_A + 100$ GeV and $\tan\beta \sim 2$ [44]. As we found in our study [38], in a general two Higgs doublet model, the discovery channel $pp \to Z\,A^0 \to l\,l\,b\,\bar{b} + X$ via $b\,\bar{b} \to Z\,A^0$ is promising for $L = 300$ fb$^{-1}$, $m_A \lesssim 400$ GeV, $\tan\beta \gtrsim 5$, $|\alpha_H| \lesssim 1$, and $m_H = m_A + 100$ GeV. The $H^0 \to Z\,A^0$ decay channel provides a good opportunity to detect $H^0$ and $A^0$ simultaneously.

The discovery potential of a neutral Higgs $\phi^0$ ($\phi^0 = h^0, H^0, A^0$) in a bottom quark gluon fusion which was studied in the previous chapter is promising for $\tan\beta > 10$ and a Higgs boson mass $\sim 1$ TeV. The $\phi^0 \to \tau\,\tau$, $\phi^0 \to \mu\,\mu$, and $\phi^0 \to b\,\bar{b}$ decay channels will provide valuable information about the Higgs-fermion couplings.

The channel $H^0 \to h^0\,h^0$ provides a good opportunity for the simultaneous observation of both $CP$-even neutral scalars. The production cross section for $H^0 \to h^0\,h^0 \to b\,\bar{b}\,\gamma\,\gamma$ is significant in the region $\tan\beta < 4$ and $2\,m_h < m_H < 2\,m_t$.

For low values of $\tan\beta$ and the mass region $m_Z + m_h < m_A < 2\,m_t$ the dominant decay mode is $A^0 \to Z\,h^0$ for the pseudoscalar Higgs boson $A^0$. At the LHC the simultaneous discovery of both $A^0$ and $h^0$ is possible through the $A^0 \to Z\,h^0 \to l\,l\,b\,\bar{b}$ channel.

Figure 5.2 shows for large integrated luminosities the entire $m_A$-$\tan\beta$ plane is accessible at the LHC [17, 37]. However for moderate values of $\tan\beta$ there is a region from $m_A =$

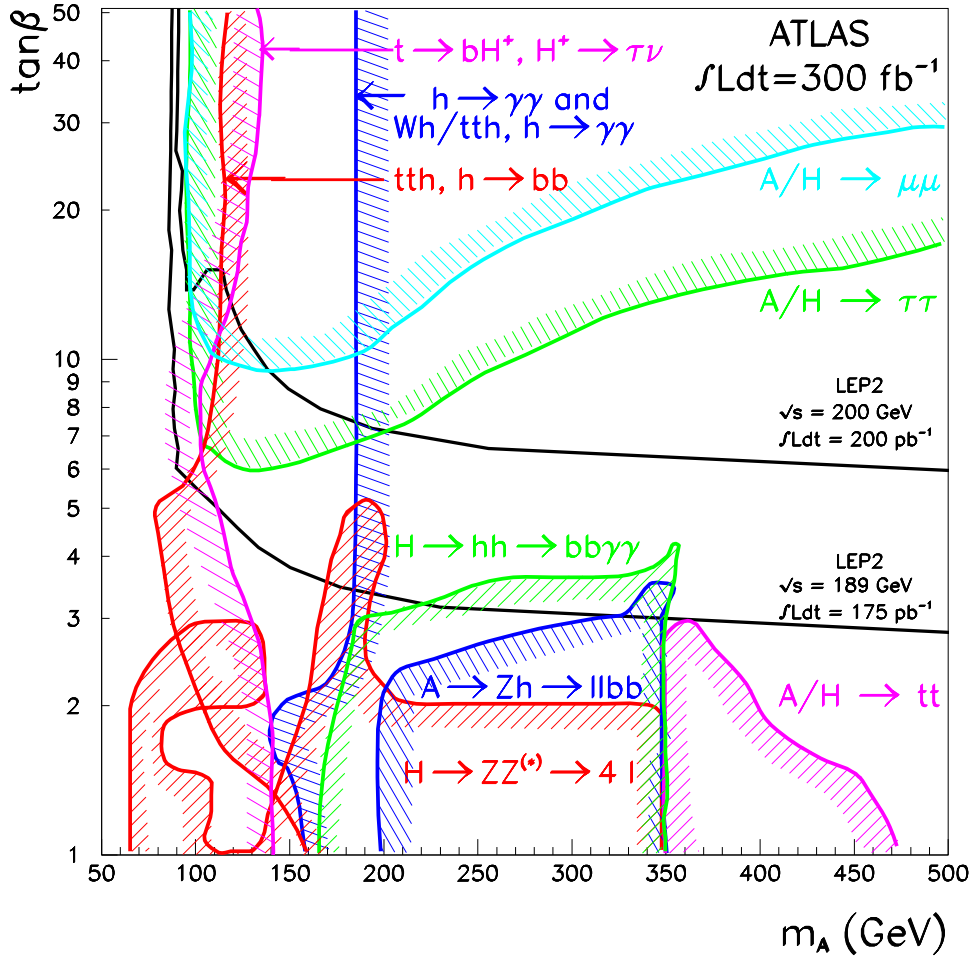


Figure 5.2: The 5 $\sigma$ contours for MSSM Higgs boson discovery through various channels in the $m_A - \tan\beta$ plane with integrated luminosity of L = 300 fb$^{-1}$ for the ATLAS detector [37].

200 GeV to higher $m_A$ values the heavier Higgs cannot be discovered at the LHC. In this region only the lightest SM like Higgs can be discovered and precision measurements of the Higgs branching ratios and other properties will be required to differentiate between the SM Higgs and the MSSM light Higgs.

The LHC is expected to come on-line in 2008 will either discover the SM Higgs boson or reveal new physics at the TeV scale.

This research was supported in part by the U.S. Department of Energy under grants No. DE-FG02-04ER41305 and No. DE-FG02-03ER46040.

# Bibliography


[1] S. L. Glashow, Nucl. Phys. **22**, 579 (1961); S. Weinberg, Phys. Rev. Lett. **19**, 1264 (1967); A. Salam in *Elementary Particle Theory: Relativistic Groups and Analyticity* (Nobel Symposium No. 8), N. Svartholm Ed. (Almqvist and Wiksell, Stockholm), 367 (1968).

[2] R. Davis, Prog. Part. Nucl. Phys. **32**, 13 (1994).

[3] Y. Fukuda *et al.* [Super-Kamiokande Collaboration], Phys. Rev. Lett. **81**, 1562 (1998) [arXiv:hep-ex/9807003].

[4] D. N. Spergel *et al.* [WMAP Collaboration], Astrophys. J. Suppl. **148**, 175 (2003) [arXiv:astro-ph/0302209].

[5] M. E. Peskin, arXiv:0707.1536 [hep-ph].

[6] M. Tegmark *et al.* [SDSS Collaboration], Phys. Rev. D **69**, 103501 (2004) [arXiv:astro-ph/0310723].

[7] M. S. Turner, arXiv:astro-ph/0207297.

[8] M. Herrero, arXiv:hep-ph/9812242.

[9] R. Barate *et al.* [LEP Working Group for Higgs boson searches], Phys. Lett. B **565**, 61 (2003) [arXiv:hep-ex/0306033].

[10] J. Alcaraz *et al.* [ALEPH Collaboration], arXiv:hep-ex/0612034. "Updated for 2007 winter conferences, 16-March-2007., http://www.cern.ch/LEPEWWG."

[11] J. F. Gunion, H. E. Haber, G. L. Kane and S. Dawson, "The Higgs Hunter's Guide."

[12] D. A. Dicus and V. S. Mathur, Phys. Rev. D **7**, 3111 (1973); M. Veltman, Acta Physics Polonica, B **8**, 475 (1977); B. W. Lee, C. Quigg and H. B. Thacker, Phys. Rev. D **16**, 1519 (1977).

[13] A. Djouadi, arXiv:hep-ph/0503173.

[14] G. 't Hooft, C. Itzykson, A. Jaffe, H. Lehmann, P. K. Mitter, I. M. Singer and R. Stora, *New York, USA: Plenum ( 1980) 438 P. ( Nato Advanced Study Institutes Series: Series B, Physics, 59)* p.135; M. J. G. Veltman, Acta Phys. Polon. B **12**, 437 (1981).

[15] S. P. Martin, arXiv:hep-ph/9709356.

[16] H. P. Nilles, Phys. Rept. **110**, 1 (1984); H. E. Haber and G. L. Kane, Phys. Rept. **117**, 75 (1985); P. Fayet, Nucl. Phys. Proc. Suppl. **101**, 81 (2001) [arXiv:hep-ph/0107228].

[17] ATLAS Detector and Physics Performance Technical Design Report, CERN/LHCC 99-14/15 (1999).

[18] CMS Physics Technical Design Report, CERN/LHCC 2006-001 (2006).

[19] K. Peters [CDF Collaborations], arXiv:0706.1278 [hep-ex].

[20] E. Witten, Nucl. Phys. B **188**, 513 (1981); S. Dimopoulos and H. Georgi, Nucl. Phys. B **193**, 150 (1981); N. Sakai, Z. Phys. C **11**, 153 (1981).

[21] K. Inoue, A. Kakuto, H. Komatsu and S. Takeshita, Prog. Theor. Phys. **67**, 1889 (1982); **68**, 927 (1982) [Erratum-ibid. **70**, 330 (1983)]; **71**, 413 (1984).

[22] H. Georgi, Hadronic J. **1**, 155 (1978).

[23] H. E. Haber, G. L. Kane and T. Sterling, Nucl. Phys. B **161**, 493 (1979).

[24] J. F. Gunion and H. E. Haber, Nucl. Phys. B **272**, 1 (1986) [Erratum-ibid. B **402**, 567 (1993)].

[25] J. F. Donoghue and L. F. Li, Phys. Rev. D **19**, 945 (1979).

[26] P. Fayet, Nucl. Phys. B **90**, 104 (1975).

[27] The LEP Higgs working group, http://lephiggs.web.cern.ch/LEPHIGGS/www/; LHWG note 2005-01.

[28] H. Baer, M. Bisset, C. Kao and X. Tata, Phys. Rev. D **46**, 1067 (1992).

[29] V. D. Barger, M. S. Berger, A. L. Stange and R. J. N. Phillips, Phys. Rev. D **45**, 4128 (1992); J. F. Gunion and L. H. Orr, Phys. Rev. D **46**, 2052 (1992).

[30] J. F. Gunion, R. Bork, H. E. Haber and A. Seiden, Phys. Rev. D **46**, 2040 (1992).

[31] Z. Kunszt and F. Zwirner, Nucl. Phys. B **385**, 3 (1992).

[32] H. Baer, M. Bisset, D. Dicus, C. Kao and X. Tata, Phys. Rev. D **47**, 1062 (1993); H. Baer, M. Bisset, C. Kao and X. Tata, Phys. Rev. D **50**, 316 (1994).

[33] H. Baer, C. Kao and X. Tata, Phys. Lett. B **303**, 284 (1993); S. Abdullin, H. Baer, C. Kao, N. Stepanov and X. Tata, Phys. Rev. D **54**, 6728 (1996).

[34] C. Kao and N. Stepanov, Phys. Rev. D **52**, 5025 (1995).

[35] S. Dawson, D. Dicus and C. Kao, Phys. Lett. B **545**, 132 (2002).

[36] S. Dawson, D. Dicus, C. Kao and R. Malhotra, Phys. Rev. Lett. **92**, 241801 (2004).

[37] E. Richter-Was, D. Froidevaux, F. Gianotti, L. Poggioli, D. Cavalli and S. Resconi, Int. J. Mod. Phys. A **13**, 1371 (1998)

[38] C. Kao and S. Sachithanandam, Phys. Lett. B **620**, 80 (2005).

[39] V. D. Barger and R. J. N. Phillips, FRONTIERS IN PHYSICS, 71, p. 592.

[40] V. N. Gribov and L. N. Lipatov, Sov. J. Nucl. Phys. **15**, 675 (1972) [Yad. Fiz. **15**, 1218 (1972)].

[41] S. Abdullin, H. Baer, C. Kao, N. Stepanov and X. Tata, Phys. Rev. D **54**, 6728 (1996).

[42] C. Kao, Phys. Rev. D **46**, 4907 (1992).

[43] J. Yin, W. G. Ma, R. Y. Zhang and H. S. Hou, Phys. Rev. D **66**, 095008 (2002).

[44] C. Kao, G. Lovelace and L. H. Orr, Phys. Lett. B **567**, 259 (2003).

[45] J. Pumplin, D. R. Stump, J. Huston, H. L. Lai, P. Nadolsky and W. K. Tung, JHEP **0207**, 012 (2002).

[46] MADGRAPH, by T. Stelzer and W. F. Long, Comput. Phys. Commun. **81**, 357 (1994).

[47] HELAS, by H. Murayama, I. Watanabe and K. Hagiwara, KEK report KEK-91-11 (1992).

[48] N. Brown, Z. Phys. C **49**, 657 (1991).

[49] H. E. Haber and Y. Nir, Phys. Lett. B **306**, 327 (1993) [arXiv:hep-ph/9302228].

[50] C. Kao, D. Dicus, R. Malhotra, and Y. Wang, University of Oklahoma Report, OKHEP-07-02.

[51] C. Kao, P. Gutierrez, S. Sachithanandam, and Y. Wang, University of Oklahoma, OKHEP-07-03.

[52] J. Campbell, R. K. Ellis, F. Maltoni and S. Willenbrock, Phys. Rev. D **67**, 095002 (2003) [arXiv:hep-ph/0204093].